This is the Accepted Manuscript version of the following article: U. Minora, D. Bocchiola, C. D'Agata et al., Glacier area stability in the Central Karakoram National Park (Pakistan) in 2001–2010: the ''Karakoram Anomaly'' in the spotlight, Progress in Physical Geography, 1-32, © The Author(s) 2016. DOI: 10.1177/0309133316643926

Glacier area stability in the Central Karakoram National Park (Pakistan) in 2001–2010: The "Karakoram Anomaly" in the spotlight

Umberto Minora[1], Daniele Bocchiola[2], Carlo D'Agata[1], Davide Maragno[1], Christoph Mayer[3], Astrid Lambrecht[3], Elisa Vuillermoz[4], Antonella Senese[1], Chiara Compostella[1], Claudio Smiraglia[1], Guglielmina A. Diolaiuti[1]

The Karakoram Range is one of the most glacierized mountain regions in the world, and glaciers there are an important water resource for Pakistan. The attention paid to this area is increasing because its glaciers remained rather stable in the early twenty-first century, in contrast to the general glacier retreat observed worldwide on average. This condition is also known as "Karakoram Anomaly". Here we focus on the recent evolution of glaciers within the Central Karakoram National Park (CKNP, area: *13,000 km^2) to assess their status in this region with respect to the described anomaly. A glacier inventory was produced for the years 2001 and 2010, using Landsat images. In total, 711 ice-bodies were detected and digitized, covering an area of 4605.9 + 86.1 km^2 in 2001 and 4606.3 + 183.7 km^2 in 2010, with abundant supraglacial debris cover. The difference between the area values of 2001 and 2010 is not significant (þ0.4 + 202.9 km^2), confirming the anomalous behavior of glaciers in this region. The causes of such an anomaly may be various. The increase of snow cover areas from 2001 to 2011 detected using MODIS snow data; the reduction of mean summer temperatures; and the augmented snowfall events during 1980–2009 observed at meteorological stations and confirmed by the available literature, are climatic factors associated with positive mass balances. Because the response of glacier area change to climate variation is very slow for large glaciers, the presence of some of the

[1]Università degli Studi di Milano, Italy
[2]Politecnico di Milano, Milano, Italy
[3]Bavarian Academy of Sciences and Humanities, Munich, Germany
[4]EvK2-CNR Committee, Bergamo, Italy

Corresponding author:
Umberto Minora, University of Milan, Via Mangiagalli, 34, Milan 20133, Italy.
Email: umberto.minora@unimi.it

largest glaciers of the Karakoram Range in this region might have delayed observed effects of such climate change so far, or alternatively, the change may not be sufficient to drive an actual area increase. In this context, improved understanding the role of debris cover, meltwater ponds, and exposed ice cliffs on debris-covered glaciers, and surging glaciers (which are also found abundant here), are required is still an issue to clarify the mechanisms behind the Karakoram Anomaly.

Keywords
Glacier inventory, Karakoram Anomaly, remote sensing, climate change, surging glaciers

1 Introduction

Glaciers are sensitive climate indicators because they adjust their size in response to changes in climate (e.g., temperature and precipitation). There is robust evidence of global glacier shrinkage over the past five decades (Vaughan et al., 2013). This is also true on a regional scale, with some exceptions. The Hindu Kush Karakoram Himalaya (HKH from hereon) displays a heterogeneous picture in this sense.

Recent observations of glacier fluctuations indicate that in the eastern and central HKH glaciers are subject to general retreat, and have lost a significant amount of mass and area in the second half of the twentieth century (Bolch et al., 2011; Salerno et al., 2008). Rapid declines in glacier area are reported throughout the Greater Himalaya and most of mainland Asia (Bolch et al., 2012; Yao et al., 2012). However, observations of individual glaciers indicate that glacier retreat rates may vary strongly between different glacial basins, and even some advancing glaciers are observed in the Karakoram Mountains (Belò et al., 2008; Bhambri et al., 2013; Diolaiuti et al., 2003; Hewitt, 2005; Rankl et al., 2014; Scherler et al., 2011). The Eastern part of the HKH is under the influence of the Indian monsoon, which brings precipitation during summer, while the Western (which includes the Karakoram range) receives most of the annual precipitation during winter and spring, as it is influenced primarily by the westerlies originating predominantly from Mediterranean and Caspian Sea regions (Bookhagen and Burbank, 2010; Fowler and Archer, 2006). This east–west variability in the predominant wind system leads to differences in glacier accumulation in the HKK, and might be one reason for the large spread in detected glacier changes within the region (Bolch et al., 2012; Kääb et al., 2012).

The estimated glacier mass balance budget in the Karakoram positively affected the 2003–2008 specific mass balance for the entire HKH region, which was calculated by Kääb et al. (2012) to be -0.21 ± 0.05 m yr^{-1} of water equivalent. This is significantly less than the estimated global average for glaciers and ice caps (Cogley, 2009; Gardner et al., 2013; WGMS, 2013). Gardelle et al. (2012) show not only balanced to slightly negative mass budgets in the Karakoram Range, but even an expansion and thickening of some glaciers in the Central Karakoram since the early twenty-first century. Hewitt (2005) reported that 33 glaciers thickened (by 5–20 m on the lowest parts of their tongues) and advanced, or at least were stagnant in this region between 1997 and 2001. The same author defined the anomalous presence of stagnant and advancing glaciers in the Central Karakoram as the Karakoram Anomaly.

The climate–glacier relation in the Central Karakoram is still not well understood, and interactions between the cryosphere, the climate, and the hydrosphere in the lower latitudes are of great interest for both global and regional purposes. Glaciers here represent a major source of water for the Indus River, upon which agriculture, human consumption, and power production rely (Bocchiola and Diolaiuti, 2013;

Mayer et al., 2010). Observations of glacier coverage and evolution are then essential to understand the role of the cryosphere in influencing the regional hydrology and water resources in this region. An in depth scientific understanding of glacier evolution in the Karakoram was hampered hitherto by the lack of systematic long-term field observations, due to the rugged topography and the complex climatology of the area. Therefore, the combination of remote sensing studies and data from field surveys is required for improving the understanding of glacier evolution in Karakoram.

In this contribution, we focus on the protected area of the Central Karakoram National Park (CKNP, $\sim$13,000 km^2) to provide an updated picture of the glacier state in the Central Karakoram and to better characterize the Karakoram Anomaly. In this regard, we produced the CKNP glacier inventory using Landsat images from 2001 and 2010. Although other glacier inventories covering the Karakoram region are available (Randolph Glacier Inventory, Arendt et al., 2014; ICIMOD glacier inventory, Bajracharya and Shrestha, 2011; GAMDAM glacier inventory, Nuimura et al., 2015), our work focuses on the specific area of the CKNP only, providing a high-resolution and very detailed inventory. We analyzed the glacier area and supraglacial debris cover change during 2001–2010. Moreover, we analyzed the snow cover area (SCA) change occurred during 2001–2011 using MODIS snow data. Eventually, we investigated the climate change occurred since 1980 by analyzing climate data from three automatic weather stations (AWS) of the Pakistan Meteorological Department (PMD).

II Study site

The HKH stretches for more than 2000 km in length from West to East, and hosts about 40,000 km^2 of ice bodies (glaciers, glacierets, and perennial ice surfaces, http://rds.icimod.org/). The economy of the HKH region relies upon agriculture, and it is highly dependent upon water availability and irrigation (Aggarwal et al., 2004; Akhtar et al., 2008; Kahlown et al., 2007). Likely more than 50% of the water in the Indus river originating from the Karakoram comes from snow and glacier melt (Immerzeel et al., 2010; Minora et al., 2015; Soncini et al., 2015).

In this study, we focus on the area of the CKNP, an extensive ($\sim$13,000 km^2) protected area in the Northern Pakistan, in the main glaciated region of the Central Karakoram (Figure 1). It was established in 2009, and $\sim$40% of this area is covered by ice. The CKNP hosts the largest glaciers of the Karakoram range (Baltoro, Biafo, and Hispar glaciers, amongst others).

The study area is under the influence of two wind systems: the monsoons in summer and the westerlies in winter. Anyway, the north-moving monsoon storms intrude only little into the Karakoram because they are mitigated by the Nanga Parbat massif to the south. Therefore, the CKNP is mainly influenced by the westerlies (Bookhagen and Burbank, 2010).

Earlier investigations of Northern Pakistan climate displayed evidence of regional behavior (Soncini et al., 2015; Weiers, 1995; Winiger et al., 2005). Most notably, Bocchiola and Diolaiuti (2013) found three homogeneous climatic regions in Northern Pakistan, one of which was called Northwest Karakoram, which includes the CKNP (Figure 1). This region displays winter and occasional spring and summer rainfall, with precipitation increasing from 150–500 mm at 1500–3000 m above sea level (a.s.l.) to more than 1700 mm at 5500 m a.s.l. The winter precipitation provides the dominant nourishment for the glaciers of the HKH (Bocchiola and Diolaiuti, 2013). High elevation snowfall is still rather unknown, due to the diffculty of obtaining reliable measurements. Some estimates from snow pits above 5000 m a.s.l. range from 1000 mm to more than 3000 mm yr^{-1}, depending upon location (Soncini et al., 2015; Wake

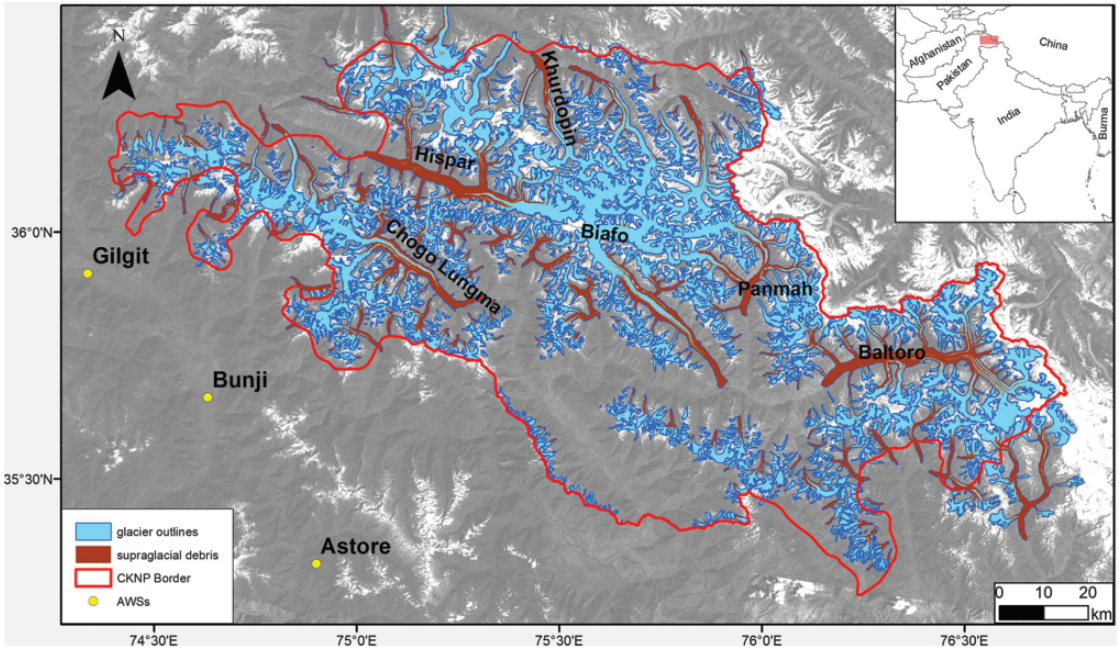

Figure 1. The CKNP, including the glacier outlines, the supra-glacial debris cover and the locations of the AWSs used in this study. CKNP: Central Karakoram National Park. AWS: automatic weather station.

et al., 1990; Winiger et al., 2005). However, there is considerable uncertainty about the spatial distribution and the vertical gradient of precipitation at high altitudes.

The glaciers in the CKNP show a large variability in size, geometry, type, and surface conditions (i.e. buried and bare ice). They belong to the Shigar and Hunza drainage basins. These are high altitude catchments with summer and annual runoff that is truly governed mostly by glacier and snow melt (Archer, 2003).

III Data sets and Methods of Analysis

1 The CKNP glacier inventory

For compilation of the CKNP glacier inventory we followed the recommendations of Paul et al. (2009), and we considered parameters such as identification code, coordinates, dates of acquisition of the image related to each glacier outline, area, length, minimum, maximum and mean elevation, mean aspect, and slope. We used Level 1 T Landsat ETM+ and TM scenes of 2001 and 2010 (Table 1) as the basis for glacier delineation.

Before proceeding to the digitization of the glacier outlines, we first increased the color contrast between the glacier bodies and the surrounding pixels by combining the near infrared and the visible bands of the TM sensor (RGB = 543). So doing, we produced false color composite (FCC) images against which we manually digitized each glacier outline separately. The minimum mapped area was 0.01 km^2 as recommended by Paul et al. (2009). The debris-free and debris-covered parts of the glaciers were not distinguished in this step. They were split afterwards by identifying the debris pixels within the glacier outlines with a supervised classification (see Section III.2).

It is worth noting that the interpretation of the glacier perimeter under debris is not straightforward (Paul et al., 2009), and thus the change

Table 1. Landsat imagery used for the analysis. Star symbol (*) indicates the reference images used for glacier delineation, the other ones were used to cross-check the results. The band combination is 543, PAN-sharpened to 15 m for Landsat 7 using the Panchromatic band (band 8).

Date	Scene identification No.	Resolution (m)	Sensor	SCAN line error	Cloud cover over glaciers (%)
21/07/2001	LE71480352001202SGS00*	15	ETM+	No	0.0
30/09/2001	LE71490352001273EDC01*	15	ETM+	No	0.0
23/07/2010	LT51480352010235KHC00*	30	TM	No	0.0
17/10/2010	LT51490352010290KHC00*	30	TM	No	0.0
18/10/2010	LE71480352010291SGS00	15	ETM+	Yes	0.0
12/08/2009	LE71480352009224SGS00	15	ETM+	Yes	0.0
22/08/2010	LE71490352010234EDC00	15	ETM+	Yes	0.1
20/09/2009	LE71490352009263SGS00	15	ETM+	Yes	0.0

ETM+: Enhanced Thematic Mapper Plus; TM: Thematic Mapper.

analysis may be problematic too. To this end, we cross-checked the position of the actual glacier border under debris with the Landsat images and the high-resolution images from Google Earth. Another crucial aspect in glacier delineation is the location of terminus position. Indeed, it can differ by several hundred meters if glacier outlines were digitized by different analysts (Paul et al., 2013). In this work, the glacier outlines for the two reference years were drawn by the same analyst, so the change analysis should be reliable. Finally, the definition of the upper glacier boundaries is also a problematic aspect. In general, steep headwalls were excluded from the mapping, similar to that by Nuimura et al. (2015). The reason is that snow cannot accumulate easily on very steep surfaces (>40°; Nuimura et al., 2015). Moreover, avalanche-fed glaciers prevail in the Karakoram, and many lack an accumulation zone as normally understood (Hewitt, 2011). We used the contour lines derived from the Shuttle Radar Topography Mission 3 DEM (SRTM3, CGIAR-CSI, 2012), to detect the steep slopes in the accumulation areas close to the glacier limits and exclude them from the inventory when there were rock exposed walls covered by thin snow layers or spotty snow patches. However, this criterion might have excluded steep areas in the accumulation zone where snow is present throughout the year, and thus the actual final glacier area might be biased by this exclusion.

Afterwards, we used a Geographic Information System (GIS) to extract topographic parameters based on the glacier outlines and the DEM. The maximum length of each glacier was derived by manually depicting a line from the highest to the lowest altitude within each glacier outline, and passing through the main flow line (according to the contour lines). The mean slope was then calculated for each glacier from elevation range and length data.

Eventually, we identified surging glaciers according to both the magnitude of their termini advance (Cuffey and Paterson, 2010), the presence of looped moraines indicating possible past surge events (Copland et al., 2003), and by comparison against the available literature (Copland et al., 2011; Hewitt, 2007; Quincey et al., 2001; Rankl et al., 2014).

2 Supraglacial debris mapping

A supervised maximum likelihood (SML) classification on the Landsat FCC image (bands 543) was used to map the supraglacial debris for the years 2001 and 2010. First, the classifier

was trained to recognize the supraglacial-debris by choosing appropriate regions of interest (ROIs). Then, the automatic classification was run against the image of 2001 and then of 2010, on the glaciers only, using the glacier masks of the respective year. So doing we obtained the supraglacial debris maps for both years. Finally, we produced the shadow maps with the same procedure to search for the locations where the glacier area was shaded. This way we were able to identify the areas of possible debris cover excluded by the classification and add them manually to the final map after cross-checking the actual presence of debris with different sources (other Landsat images, Google Earth).

3 Glacier outline and error assessment

When dealing with the production of glacier inventories through satellite images, inaccuracies may occur due to classification errors. These depend upon the image resolution and the meteorological and environmental conditions at the time of acquisition, namely cloud- and snow-cover, presence of shadows and debris, hampering ice detection. In the following, the impacts of different sources of error are discussed.

Georeferencing error. The georeferencing accuracy is optimized by the United States Geological Survey (USGS) by means of a correction process based both upon ground control points (GCPs, taken from the 2005 Global Land Survey) and the SRTM DEM (Landsat7 Handbook, 2013). The SRTM DEM is thought to have good accuracy (Falorni et al., 2005). The true geolocation is not too critical for our analysis because our Landsat data are processed in the same way by the USGS.

Linear resolution error (LRE). Image resolution influences the accuracy of glacier mapping. Following Vögtle and Schilling (1999) and Citterio et al. (2007), the final planimetric precision value was assessed considering the uncertainty due to the sources (satellite images). The area precision for each glacier was evaluated by buffering the glacier perimeter, considering the area uncertainty. According to O'Gorman (1996), the LRE should be half the resolution of the image pixel, i.e., in our case 7.5 m for the 2001 scenes (because the scenes were PAN-sharpened), and 15 m for the 2010 scenes. This error may be too low for debris pixels, because glacier limits are more difficult to distinguish when ice is covered by debris (Paul et al., 2009). Therefore, we set the error for debris pixels to be three times that of clean ice. The precision of the whole CKNP glacier coverage was estimated as the root squared sum (RSS) of the buffer areas for 2001 and 2010:

$$AE_{yr} = \sqrt{\sum_{i=1}^{N} (p_i * LRE_{yr})^2} \qquad (1)$$

where AE_{yr} is the areal error of year 2001 or 2010, p_i is the i^{th} glacier perimeter, LRE_{yr} is the LRE of year 2001 or 2010, and N is the total number of glaciers in the inventory. Finally, the total error in area change ($AE_{\text{area change 2001–2010}}$) was then calculated as the RSS of the areal errors related to each glacier in the 2001 and 2010 (AE_{2001} and AE_{2010}):

$$AE_{area\ change 2001-2010} = \sqrt{AE_{2001}{}^2 + AE_{2010}{}^2} \qquad (2)$$

Error depending on specific scene conditions. Seasonal snow, cloud cover, presence of shadows, and debris can introduce errors in glacier area determination. The scenes were selected to display minimum snow and cloud over the glaciers. In case these features were still present, and to deal with the interpretation of invisible glacier boundaries in cast shadows and the actual perimeter under debris, we used images from different sources (i.e. Landsat and Google Earth) and dates (see Table 1), which enabled us

to cross-check the actual glacier limits and to minimize any possible interpretation error.

Error depending on operator's misinterpretation. Because glacier outlines are mapped manually, errors may occur due to the operator's misinterpretation of the image pixels. Nevertheless, although several semi-automated techniques for mapping debris-covered glaciers have been proposed (Paul et al., 2004; Shukla et al., 2010, amongst others), they all require more complex processing, an accurate DEM and final manual editing (Paul et al., 2013). We therefore preferred the manual approach, trying to reduce any possible misinterpretation error through the choice of an expert eye for the digitization, and a second-round check on the final mapping. Note that this has nothing to do with the automatic classification of the supraglacial-debris, as this was performed after glacier borders were drawn (see Sections III.1 and III.2).

4 Snow cover data

We used MODIS MOD10A2-V5 snow product (Hall et al., 2006) to investigate snow-cover variability during 2001–2011 in the CKNP. These data are freely available at the National Snow and Ice Data Center website (NSIDC, 2013). They contain information of maximum snow cover extent over an eight-day period (henceforth the use of a specific "Julian day" refers to the same Julian day and seven days after from hereon). Pu et al. (2007) reported an average of 90% overall accuracy during 2000–2006 on the Tibetan Plateau using the same product compared with in-situ Chinese snow observations.

We set a threshold for cloud cover to reduce cloud noise in our dataset. We chose 50% cloud cover as the best tradeoff between data reliability and availability, in line with other studies (e.g. Parajka and Blöschl, 2008).

Because most of the available dataset was not investigated by the NSIDC group for quality check at the time of our analysis, we decided to work only with those images flagged within the NSIDC quality assessment as "INFERRED PASSED". This issue led to the larger loss of data in our time window, especially during winter, when comparatively few images could be retained. We then chose to analyze snow cover dynamics during the ablation season only (from June 18 to September 30), using a total of 37 images. The late summer SCA was used to calculate the late summer Snow Line Altitude (SLA) at the end of the ablation season. We used Julian day 273 as the reference day for late summer SCA, according to the period (i.e., end of the ablation season), and to snow cover minima detected at this day. When this date was not present in the dataset, we used the closest previous date (Table 2). We then inspected the available winter snow coverage to insure the capture of the largest snow cover (SCA_{Max} further on, see Section IV.2).

The results are compared with those of Thair et al. (2011), who studied snow cover in the Hunza basin, north of the CKNP. Because they divided SCA data and trends in three altitude belts (A, B, and C), we divided our dataset much the same way (see Table 9 in Section IV.2). To provide a meaningful comparison between different years, we compared snow cover at fixed dates. Within the available database of reasonably clear images we chose a number of dates when images were available for several years. We carried out a linear regression in time of snow cover data for each of these belts to analyze SCA trends over time.

Finally, we validated the MODIS snow product by comparison with several Landsat satellite images of the same period. The comparison and its results are detailed in Section IV.

5 Climate data analysis

Monthly averaged meteorological variables were provided by the Pakistan Meteorological Department (PMD), derived from measurements

Table 2. Julian days used to calculate late summer SLA according to data availability.

Year	2001	2002	2003	2004	2005	2006	2007	2008	2009	2010	2011
Julian day	273	241	217	273	201	169	273	273	273	273	273

Table 3. Details for the AWSs used in the study, with seasonal averages (1980–2009) of precipitation amounts and air temperature.

AWS	North (°)	East (°)	Altitude (m a.s.l.)	Ave P_{JFM} (mm)	Ave T_{JFM} (°C)	Ave P_{AMJ} (mm)	Ave T_{AMJ} (°C)	Ave P_{JAS} (mm)	Ave T_{JAS} (°C)	Ave P_{OND} (mm)	Ave T_{OND} (°C)
Astore	35.20	74.54	2168	167	0.5	167	13.8	74	19.3	76	5.8
Bunji	35.40	74.38	1372	26	8.6	66	22.0	51	26.8	18	11.9
Gilgit	35.55	74.20	1460	23	7.4	61	20.6	37	25.0	17	10.1

Average precipitation and average air temperature per season (JFM, AMJ, JAS, OND) are reported as Ave *P* and Ave *T*, respectively.

at a number of stations in North Eastern Pakistan during 1980–2009. Data from the three closest AWSs to the CKNP area, namely Gilgit, Bunji, and Astore (from north to south, Figure 1 and Table 3) are used for this study.

The altitudes of the AWSs range from 1372 m a.s.l. (Bunji) to 2168 m a.s.l. (Astore), which is rather low in comparison with the hypsography of the CKNP. Given the large precipitation lapse rates expected within the upper Karakoram (Bocchiola et al., 2011; Winiger et al., 2005; Wulf et al., 2010), precipitation at these low stations may not be fully representative of precipitation in the CKNP. Data from AWSs at higher altitudes (e.g. Askole, 3015 m a.s.l., and Urdukas, 3926 m a.s.l., installed by Ev-K2-CNR, see Bocchiola et al., 2011) are available, but they cover a very short period (2005–now), and display large lack of data. Therefore, little information is available within the CKNP that we know of, so we could only rely upon data from the three selected AWSs. In spite of the considerable vertical gradients within the area (temperature and precipitation, the latter more uncertain), relative variations observed at the selected stations may be taken as representative of variation also at the highest altitudes, at least in a first approximation.

The main parameters for the climate analysis are the monthly amount of precipitation, P_m (mm), the monthly number of wet days, D_w, and the monthly averages of the maximum and minimum daytime air temperatures, T_{max} (°C) and T_{min} (°C). P_m provides the hydrological input on the area, while D_w indirectly indicates the frequency (or average duration) of precipitation events (days with rainfall/snowfall). Unfortunately, no snow gauges are available in the PMD database, so no direct inference can be made about snow amount and snow water equivalent (SWE), neither splitting of precipitation into either rainfall or snowfall was possible, and P_m is labeled as "monthly amount of precipitation". High altitude snowfall in this area seems still rather unknown. Some estimates from accumulation pits above 4000 m a.s.l. range from 1000 mm to more than 3000 mm, depending on the site (Winiger et al., 2005), and the authors here found ca. 1000 mm per year during 2009–2011 in the Baltoro glacier area at ca. 6000 m a.s.l. (Soncini et al., 2015). However, there is considerable uncertainty about the behavior of precipitation at high altitudes, and lack of snowfall data may lead to underestimation of total precipitation. Here, upon analysis of the average minimum winter temperature T_{min}

(below 0°C most of the time at the sites), we may assume that water under snowfall is included and P_m is a measure of total precipitation.

The maximum and minimum daytime temperatures (T_{max} and T_{min}) provide an indication about the temperature characteristics in the investigated periods (i.e., arrival and duration of heat waves). Annual (Y) and seasonal (SEA) values of the variables are also derived and used in the analysis: $P_{m,\ Y/SEA}$ is the sum of the monthly values during a year/season; $D_{w,\ Y/SEA}$ represents the mean of monthly values during a year/season; and $T_{max,\ Y/SEA}$ and $T_{min,\ Y/SEA}$ are calculated as the mean of monthly values during a year/season.

The data are investigated for trends using linear regression (LR) analysis and the non-parametric Mann–Kendall (MK) test, both traditional and progressive (backward-forward). The significance of LR during the period of observations is given by a p-value ($p = 5\%$, e.g., Jiang et al., 2007). Multiple trends could be identified in the time series analysis, e.g., by assessing slope changes (see Bocchiola, 2014; Seidou and Ouarda, 2007). However, in view of the relative shortness of the series, a single slope regression analysis was carried out. The MK test (Mann, 1945; Kendall, 1975) is widely adopted to assess the significance of trends in time series (Bocchiola et al., 2008; Yue and Wang, 2002; Zhang et al., 2000). It is a non-parametric test, less sensitive to extreme values, and independent from the hypothesis about the nature of the trend (e.g., Wang et al., 2005). Here the MK test was applied to raw data, without pre-whitening, according to Yue and Wang (2002). Upon visual inspection of the data, which would not display evident break points or unexpected abrupt changes, and given that no modification of the stations' status was labeled by PMD, we did not carry out any homogenization procedure.

Further on, we tried to verify the hypothesis that the temperature evolution in the Karakoram is related to warming at global or hemispheric scale. To do so, we investigated the correlation between global temperature anomalies, ΔT_G (calculated according to Brohan et al., 2006), and T_{min} and T_{max} at the AWSs. Also, we investigated the correlation of the weather variables against the anomaly (vs. long term average) of the Northern Atlantic Oscillation (NAO) index (Hurrell, 1995; Jones et al., 1997; Osborn, 2004, 2006), during 1980–2009. Former studies demonstrated the existence of correlation between the NAO and the Karakoram climate, most notably with precipitation (Archer and Fowler, 2004). We therefore evaluated the (linear) correlation between i) local air temperatures and ΔT_G, and ii) the investigated weather variables and the NAO index. As a representative parameter of the region, the averaged values between the three AWSs have been used.

IV Results

1 Glacier changes during 2001–2010

According to our inventory, the CKNP hosts 711 glaciers (see Table 5). Their total area in 2001 is 4605.9 $\pm$ 86.1 km^2, $\sim$35% of the study site. This area represents $\sim$30% of the glacier surface of the entire Karakoram Range within Pakistan (total area from Bajracharya and Shrestha, 2011). The biggest glacier is 604 km^2 (Baltoro Glacier), while the mean glacier size is 6.5 km^2. We divided the glaciers into size classes following Bhambri et al. (2011) (Table 4).

Only 17 glaciers fall within the largest size class (>50 km^2), but they cover more than half of the glacierized surface of the park. Glaciers in the smallest classes (<1 km^2) account for ca. 61% in number, while covering only 3.5% of the glacier area. Glacier minimum elevation (i.e., glacier termini elevation) is between 4500 and 5000 m a.s.l. on average, with few larger glaciers reaching farther down (between 3000 and 3500 m a.s.l., Table 5).

Smaller glaciers (<1 km^2) tend to have higher termini location, similar to what is observed in other glaciated regions, including, for example,

Table 4. Number of glaciers and area distribution within the study region, sorted according to glacier size for 2001.

Size class (km^2)	Number of glaciers	Number of glaciers (%)	2001 glacier area (%)
<0.5	291	40.9	1.4 ± 0.5
0.5–1.0	140	19.7	2.1 ± 0.5
1.0–2.0	118	16.6	3.7 ± 0.4
2.0–5.0	75	10.3	5.2 ± 1.9
5.0–10.0	36	5.3	5.3 ± 2.3
10.0–20.0	18	2.5	5.4 ± 2.8
20.0–50.0	16	2.3	11.4 ± 2.9
>50.0	17	2.4	65.4 ± 2.8
Total	711	100	100 ± 1.9

the Alaska Brooks Range (Manley, 2005), the Swiss glaciers (Kääb et al., 2002), the Cordillera Blanca (Racoviteanu et al., 2008), and the Italian Alps (Diolaiuti et al., 2012).

From the glacier hypsography, we observe that glaciers range in elevation from 2250 to 7900 m a.s.l. (Figure 2). Small glaciers with areas smaller than 1 km^2 are restricted to elevations above 3500 m a.s.l. Their elevation range is not very high, but some of them are even found up to 7000 m a.s.l. (Figure 3).

Most of the large and prominent glaciers instead originate above 7000 m a.s.l., and have a wide elevation range. Further, the minimum elevation reached by some of these large glaciers is much lower than in the Greater Himalaya of India and Nepal (Hewitt, 2005).

We found a significant correlation ($\rho = 0.5$) of area vs. altitudinal range (i.e., maximum minus minimum elevation). Glaciers with smaller vertical extent (i.e., maximum elevation close to the average) feature smaller areas. This is because they have small mass exchanges and therefore they cannot produce long tongues. Also, they can only survive in elevation where accumulation is secured.

In the available literature (Bocchiola et al., 2011; Mayer et al., 2006; Mihalcea et al., 2008; Minora et al., 2015; Soncini et al., 2015), the equilibrium line altitude (ELA) for CKNP glaciers is placed between 5200–5300 m a.s.l. According to Braithwaite and Raper (2009), the ELA can be estimated from the median glacier elevation with an error of ±82 m. The median glacier elevation derived from our inventory is 4985 m a.s.l. Rather than an indication of negative mass budgets, this discrepancy with the literature value is more likely due to i) the exclusion of the steep headwalls from the upper glacier limits in our inventory (which entails a lower value of median elevation), and ii) the fact that many glaciers are significantly nourished by avalanches and hence have small accumulation regions. As a best approximation, the actual ELA of the CKNP glaciers could be placed between 5000 and 5200 m a.s.l. (Figure 2).

In 2010, the glacier area of CKNP was 4606.3 ± 183.7 km^2, slightly more than in 2001. Table 6 shows glacier data from 2001 and 2010, and it highlights some important changes between the two years. Because some glaciers changed their size class during 2001–2010, the analysis of the area changes was performed considering the glaciers to belong to the same size classes of 2001 for both years (Table 6).

The analysis shows that the total glacier surface is rather stable during 2001–2010. The total area change is 0.4 ± 202.9 km^2; 137 glaciers compared to the entire sample of more than 700 glaciers changed in area (namely the 19% of all the glaciers). Glaciers increasing their areas since 2001 account for an area gain of +9.2 ± 118.5 km^2, while the loss was -8.8 ± 164.7 km^2.

In spite of the overall stable situation some glaciers showed considerable changes. Some of these are surge-type glaciers (Table 7). We found a maximum advance of 2200 m in the study period (Shingchukpi Glacier, Figure 4(a)). Examples of important advances are also given by other tributaries of the Panmah Glacier (South Chiring Glacier, Figure 4(b), and Second Feriole Glacier), which have experienced surges in 2001 and 2005 (Hewitt, 2007), now

Table 5. Glacier number and area distribution with respect to glacier termini elevation based on the 2001 inventory data.

Minimum glacier altitude (m)	Glacier number	Cumulative area (km^2)	% of total area	% of total number
2000–2500	3	105.8 ± 7.2	2.3 ± 6.8	0.4
2500–3000	12	633.8 ± 29.5	13.8 ± 4.7	1.7
3000–3500	24	2152.5 ± 74.6	46.7 ± 3.5	3.4
3500–4000	83	950.3 ± 29.3	20.6 ± 3.1	11.7
4000–4500	229	449.2 ± 7.1	9.8 ± 1.6	32.2
4500–5000	268	258.6 ± 4.2	5.6 ± 1.6	37.7
5000–5500	77	37.0 ± 0.4	0.8 ± 1.0	10.8
>5500	15	18.8 ± 0.5	0.4 ± 2.6	2.1
Total	711	4605.9 ± 86.1	100 ± 1.9	100

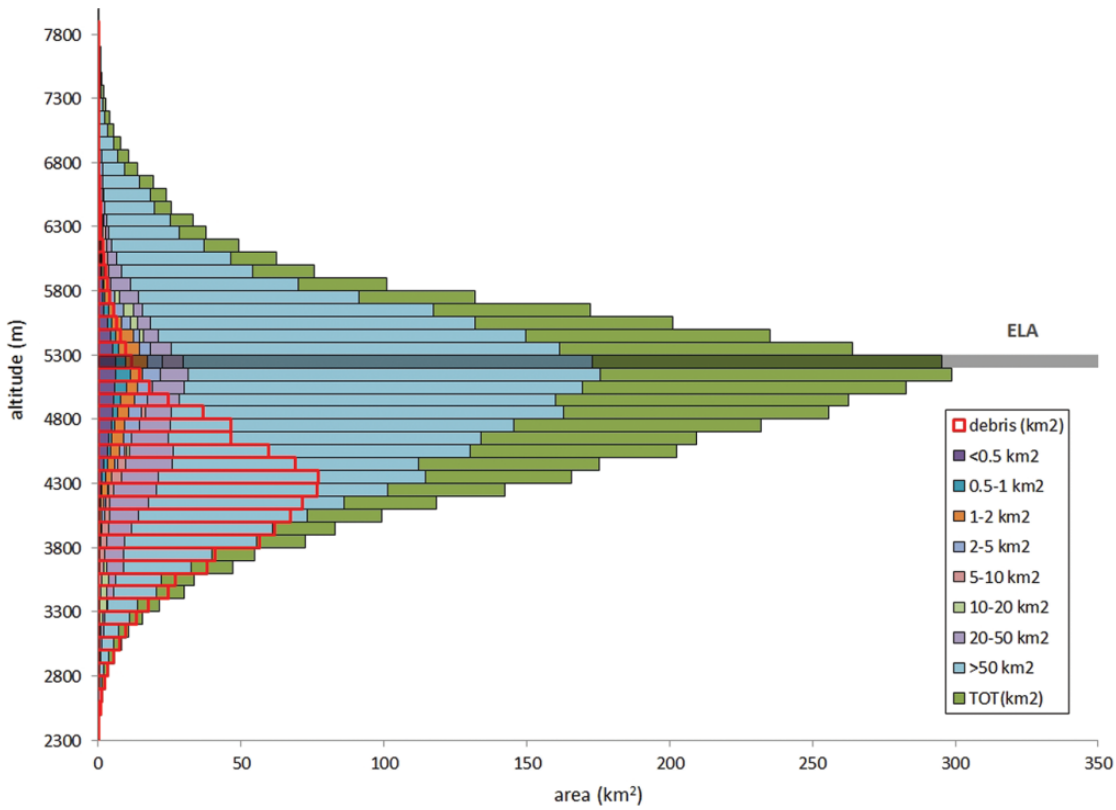

Figure 2. Hypsography of glacier area distribution per size class and debris-cover by 100 m elevation bins (based on 2001 glacier mask). Elevation data are based on the SRTM DEM of 2000. The gray bar represents approximate placement of ELA. ELA: Equilibrium Line Altitude.

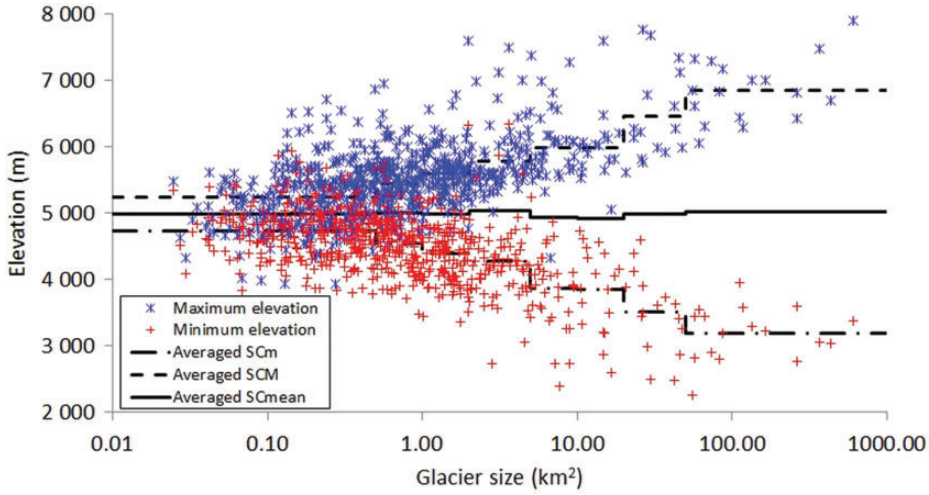

Figure 3. Minimum and maximum elevation versus area size (2001). Values for discrete size classes are also given. Notice the logarithmic scale for glacier size. SC: size class; m: minimum, M: maximum.

Table 6. Area coverage of glaciers within the CKNP according to satellite images (2001 and 2010) (columns 2 and 3). Surface area changes of the CKNP glaciers during 2001–2010 (columns 4 and 5).

Size class (km^2)	2001 area (km^2)	2010 area (km^2)	ΔA 2001–2010 (km^2)	ΔA 2001–2010 (%)
<0.5	66.2 ± 0.4	66.1 ± 0.7	−0.1 ± 0.8	−0.1 ± 1.2
0.5–1.0	97.4 ± 0.5	97.7 ± 1.0	0.2 ± 1.2	0.2 ± 1.2
1.0–2.0	170.4 ± 0.8	170.5 ± 1.6	0.03 ± 1.8	0.02 ± 1.0
2.0–5.0	239.9 ± 4.6	242.5 ± 8.7	2.6 ± 9.9	1.1 ± 4.2
5.0–10.0	246.2 ± 5.7	246.7 ± 11.9	0.4 ± 13.1	0.2 ± 5.2
10.0–20.0	248.1 ± 7.0	251.1 ± 14.8	3.0 ± 16.3	1.2 ± 6.5
20.0–50.0	525.6 ± 15.2	525.4 ± 32.0	−0.2 ± 35.4	−0.04 ± 6.7
>50.0	3012.1 ± 84.1	3006.5 ± 179.7	−5.6 ± 198.4	−0.2 ± 6.6
Total	4605.9 ± 86.1	4606.3 ± 183.7	0.4 ± 202.9	0.01 ± 4.4

protruding far onto the main trunk of the Panmah Glacier. The overall contribution of the advancing surge-type glaciers to the CKNP area gain is 2.6 km^2, about 28% of the total area gain in 2010 with respect to 2001.

Finally, the total supraglacial-debris coverage was 946.2 ± 57.5 km^2 in 2001, and 1054.6 ± 117.3 km^2 in 2010, i.e., about 20% of the total ice covered area (see also Figure 1). When considering only the ablation area, the relative coverage is up to 31%. The supraglacial debris covers 20–27% of glaciers in the size classes larger than 2 km^2 (size classes 4–8, see Tables 4 and 6), with maximum in size class number 7 (20–50 km^2) (Figure 5).

According to our calculation, the debris cover increased by108.4 ± 130.6 km^2. Despite such error, this increment can be clearly observed on specific glaciers, as for the Chogo Lungma Glacier (Figure 6). The maximum supraglacial-debris cover is found at 4300 m a.s.l. (see also Figure 2).

Table 7. List of advancing surging glaciers in the CKNP from 2001 to 2010.

Glacier ID	Name	Latitude (°)	Longitude (°)	Advance (m)	Area gain (km^2)
276	Second Feriole Glacier	35.86	76.00	1800	0.8
534	Shingchukpi Glacier	35.90	76.02	2220	1.7
601	Skorga Glacier	36.24	75.76	375	0.2
616*	Maedan Glacier	35.93	76.03	900	0.8
616*	Drenmang Glacier	35.97	76.02	800	1.2
642	Unnamed	36.12	75.23	310	0.06
673	Unnamed	36.09	75.88	915	0.8
706	Kunyang Glacier	36.14	75.11	600	2.4

*Glacier code refers to the Panmah Glacier, of which these glaciers are tributaries.

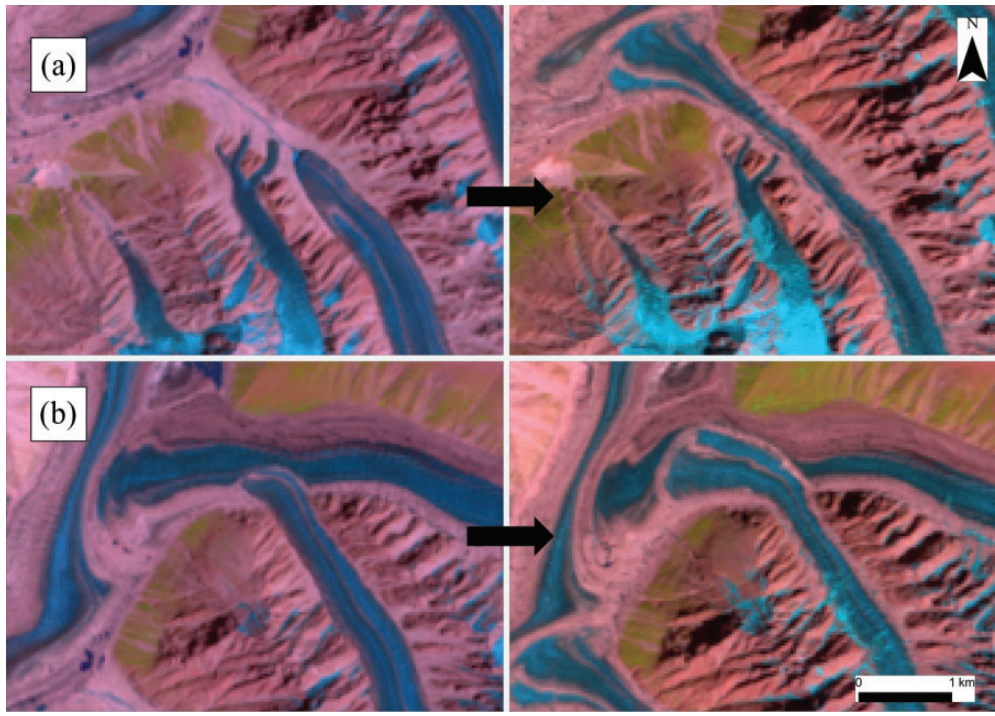

Figure 4. Comparison of Shingchukpi Glacier's (a) and South Chiring Glacier's (b) positions in 2001 (left) and 2010 (right).

2 Snow cover validation and variability

Several Landsat TM and ETM+ scenes were processed to provide high-resolution (30 m) snow maps to be compared with the MOD10A2 product used for the snow cover analysis (Table 8). The snow maps were derived using the Normalized Difference Snow Index (NDSI), which combines the reflectance values of band 2 and 5 (b2, b5) of the Landsat satellite as:

$$NDSI = \frac{b2 - b5}{b2 + b5}. \quad (3)$$

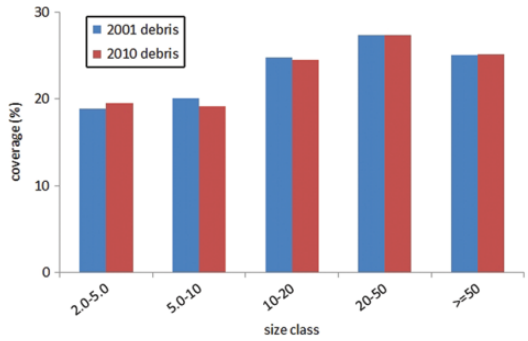

Figure 5. Supraglacial-debris coverage according to glacier size class. Glaciers smaller than 2 km^2 are excluded from the graph because debris coverage was negligible.

As our snow cover analysis only referred to the ablation season, we selected Landsat scenes from the beginning of July to the first days of October. Moreover, we resampled the Landsat snow maps to match the resolution of the MOD10A2 product (500 m) to evaluate the effect of the spatial resolution on the comparison. The resampling was done using the majority method, which assigns the most common value amongst the original pixels in a specific window to the new larger pixel.

The relative error ranges from 1 to 38% overall, but a difference is seen if i) Landsat TM and ETM+ scenes are considered separately, and ii) the resampled Landsat snow map is considered instead of the original resolution (Figure 7). In the first case, the relative error is 1–20% when considering the ETM+ sensor, while it is 7–38% for the TM sensor. The comparison is also done with the older Landsat 5 satellite, because of the SCAN-line corrector failure after April 2003 of the Landsat 7 satellite, which caused data loss in the images recorded after this date. The resampled Landsat snow maps might provide a better comparison with the MODIS product due to the identical pixel dimension, which mimics a similar decision strategy as for a MODIS pixel, depending on the used threshold for the MOD10A2 product. The relative error is lower in the resampled snow map than in the original data. In particular, the relative error range (0–14%) is smallest when comparing the resampled snow maps derived from the ETM+ sensor.

It is worth remembering that the MOD10A2 product represents an eight-day snow cover bundle, so the differences can also depend on the different time resolution of the two datasets (1 day for the Landsat satellites, and 8 days for the MOD10A2). In particular, if the Landsat acquisition date coincides with a snowfall event, or is just before, major differences might occur. Moreover, the way the MOD10A2 product is generated by the NSIDC minimizes cloud-cover extent, such that a cell needs to be cloud-obscured for all days in order to be labeled as cloud (nsidc.org). This makes this product preferable to the MOD10A1 daily product (Wang et al., 2008), and does not require additional cloud correction to be used.

The average SCA_{LS}, or snow covered area in late summer, during 2001–2011 was investigated with respect to altitude bins of 1000 m, refined into 500 m bins from 3000-6000 m a.s.l., where most of the snow dynamics likely occurs and ELA is expected to dwell (Figure 8). The aspect (8 bins of 45°) is also analyzed to study the variability of snow cover with orientation. A considerable part of the SCA is laid between 4000 and 6000 m a.s.l. as expected, quite rapidly decreasing for lower and higher altitudes. Especially in the lower altitudes the southern slopes show clearly less snow cover than the other orientations.

On average, 88% of SCA in late summer is situated between 4000 and 6000 m a.s.l. ($SCA_{LS}^{\%}$) (Figure 9), thus demonstrating how snow dynamics is most important in this altitude bin, and that such range of altitude is utmost critical, also in view of potential changes of snow cover in response to climate change. From the shape of the SCA_{LS}* curve (2001–2011 average snow cover area in late summer), it is

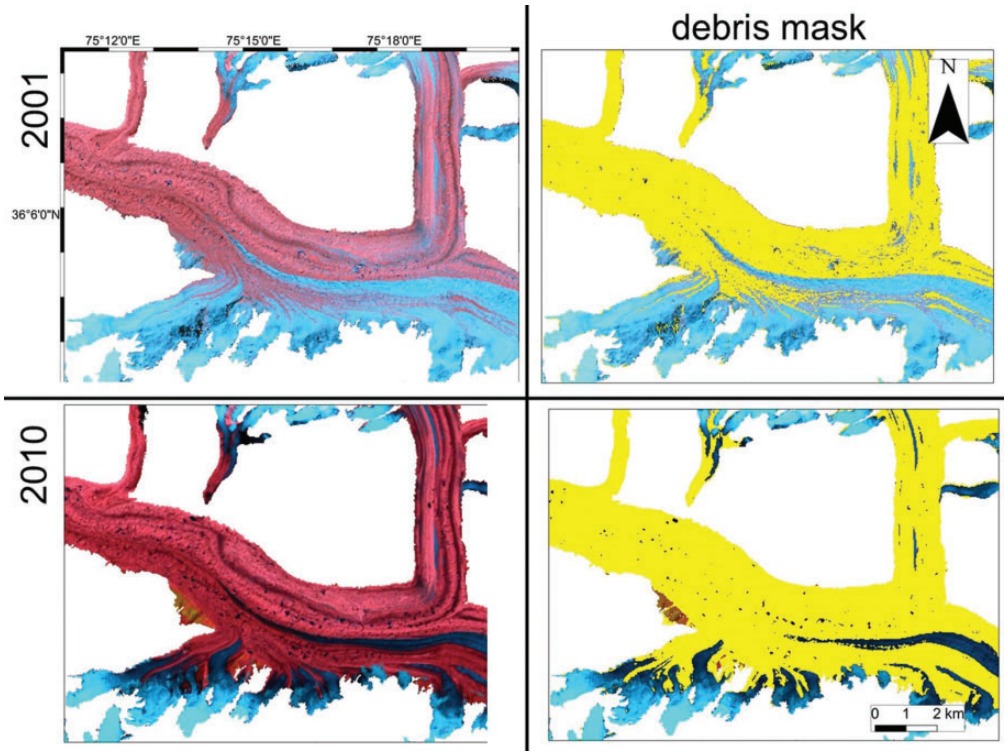

Figure 6. Supraglacial debris coverage for 2001 (upper figures) and for 2010 (lower figures) for a portion of the Chogo Lungma Glacier. FCC images (left), and debris coverage in yellow (right) are shown.

Table 8. Statistics of snow cover area obtained from Landsat NDSI and MOD10A2 snow product for different years. Landsat snow maps are also presented in the 500 m pixel resampled version (majority method).

	Path/ row	Date	ETM+ (km^2)	TM (km^2)	MOD10A2 (km^2)	Relative error (%)	ETM+ 500 m (km^2)	TM 500 m (km^2)	Relative error (%)
ETM+	148035	July 2001	2798		2904	4	2755		5
	149035	September 2001	3869		4625	20	4646		0
	148035	August 2002	3211		3257	1	3690		-12
	149035	August 2002	2963		3198	8	3722		-14
TM	148035	October 2008		3498	4817	38		4270	13
	149035	September 2008		4410	4853	10		4848	0
	148035	August 2009		3251	3469	7		4033	-14
	149035	August 2009		2812	3353	19		3556	-6
	149035	October 2010		3544	4888	38		3526	39

clearly seen how on average, above 5500 m a.s.l. and up to 8000 m a.s.l., snow cover in late summer is stable at about 85% of the maximum seasonal value. Below this altitude, SCA_{LS}* decreases quickly. $SCA_{Max}{}^{\%}$ indicates the contribution to snow cover of each altitude belt

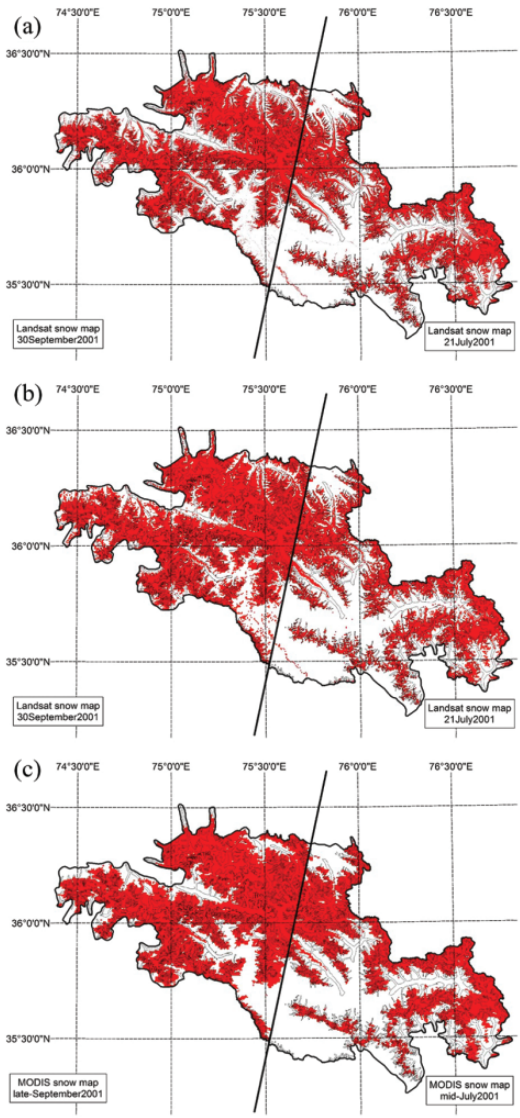

Figure 7. Snow cover areas (in red) for the CKNP in 2001. The black line in the center marks the edge of the two images used to cover the study area (left: July; right: September). SCA derived from (a) Landsat 7 (41% in July and 61% in September); (b) Landsat 7 resampled to 500 m (40% in July and 73% in September) and; (c) MOD10A2 (42% in July and 72% in September.

during winter time, i.e., when SCA reaches its largest value. The comparison of $SCA_{LS}{}^{\%}$ against $SCA_{Max}{}^{\%}$ quantifies the relative importance of the loss of snow cover at the end of summer in each belt, i.e., as quantified by SCA_{LS}*. Notably the greatest cumulated SCA loss (*i.e.* the vertical distance between $SCA_{LS}{}^{\%}$ and $SCA_{Max}{}^{\%}$) is reached towards an altitude of ca. 5000–5300 m a.s.l. (ca. 20%), with a decrease above. This means that areas above this belt tend to have a continuous snow cover throughout the year. We therefore placed the late summer snow line at an altitude nearby 5300 m a.s.l., which roughly corresponds to the ELA. This is consistent with the pattern of SCA_{LS}*, displaying swift increase above between 5000 and 5500 m a.s.l.

We finally subdivided our SCA dataset into three elevation bands (A, B, C, see Table 9) according to Tahir et al. (2011), for benchmark against their findings (i.e., increased SCA in the Hunza basin in the same period). Table 8 reports the rate of variation in time, or slope, of the snow coverage within each of the three belts. Slope is the value of the rate of variation estimated using linear regression analysis, expressed in km^2 per year. $Slope_{SCA\%}$ is the rate of variation expressed as a percentage of the initial SCA (in 2001) per year. A slight increasing trend of snow cover through time is visible in all the elevation belts (Figure 10). In belt A, a gain of $+0.09\ km^2\ yr^{-1}$ (or 2% of snow cover area per year), was observed. In belt B, snow cover area increased by $+2.35\ km^2\ yr^{-1}$, or $+0.6\%\ yr^{-1}$. Belt C has increasing snow cover of $+14.9\ km^2\ yr^{-1}$, or $+0.2\%\ yr^{-1}$.

3 Climate trends

The results of the trend analysis of climate are shown in Table 10 and Figures 11 to 13, where the most significant trends are highlighted. The progressive MK test was carried out whenever both MK and LR tests showed non-stationarity, and the results are also shown in Table 10. Precipitation P_m demonstrates a substantial stationary behavior, i.e., no significant change is seen in

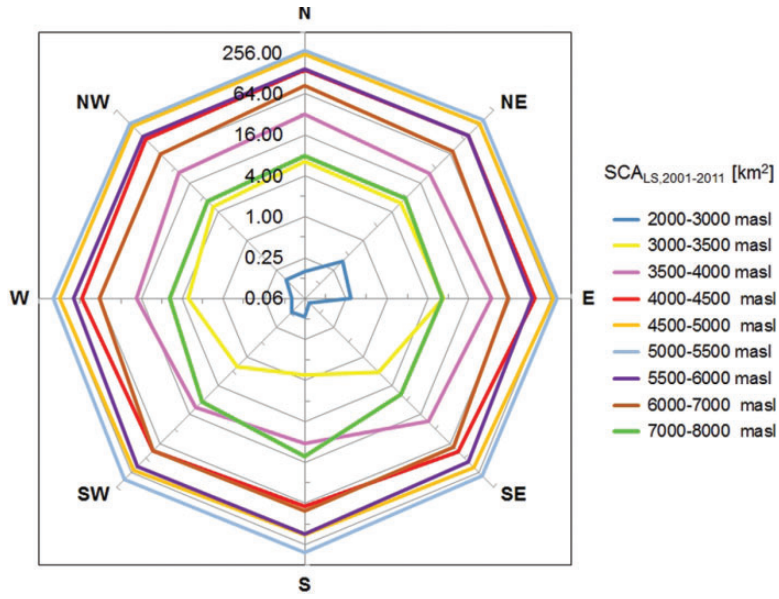

Figure 8. Average snow covered area in late summer, $SCA_{LS,}$ as per altitude bins, and aspect. Logarithmic scale (base 2) is used to enhance small snow covered areas at very low (and very high) altitudes. SCA: snow cover area.

the area. Concerning the number of wet days (D_w), increasing values are found in Gilgit (yearly, Y, since 2001, JFM, with no clear onset), i.e., there is a significant increase of the number of yearly (and winter) precipitation events (Figure 10). In Astore, significant increase of D_w is found in summer months (JAS) via the LR test. The minimum temperature T_{min} increases significantly in Astore for winter and spring (JFM, AMJ, since 1999–2002) and in Bunji for all periods except in summer (Y, JFM, AMJ, OND, since 1997–2003). In Gilgit, T_{min} decreases significantly during summer (JAS, since 1986). The maximum temperature T_{max} increases significantly yearly, in fall and winter in Astore (Y since 1998, JFM since 2000). Also in Gilgit, significant T_{max} increase is observed for most periods (Y, JFM, since 1995, OND, since 1991), while Bunji shows a significant T_{max} increase only in winter (JFM, since 1997).

In Table 10 we also report the results of the correlation analysis against global drivers of climate. The minimum air temperature T_{min} is significantly positively correlated with respect to ΔT_G yearly, in winter and spring. The maximum air temperature T_{max} is significantly positively correlated against ΔT_G yearly, and seasonally, especially in fall and winter. Concerning the NAO index, P_m shows a significant, albeit small correlation (negative vs. Y, and positive vs. JAS and OND). The duration of wet periods D_w is significantly shorter for higher NAO anomalies, unless during Spring. The minimum temperature T_{min} is negatively correlated to NAO during winter and spring. T_{max} is negatively correlated to NAO (Y, JFM, AMJ).

V Discussion

According to our inventory, the glaciers of the CKNP were rather stable in terms of surface during 2001–2010. This is in contrast to the evolution of most mountain glaciers outside the Polar Regions, which experienced a general retreat on average (Vaughan et al., 2013). In this section we relate such stability with the results

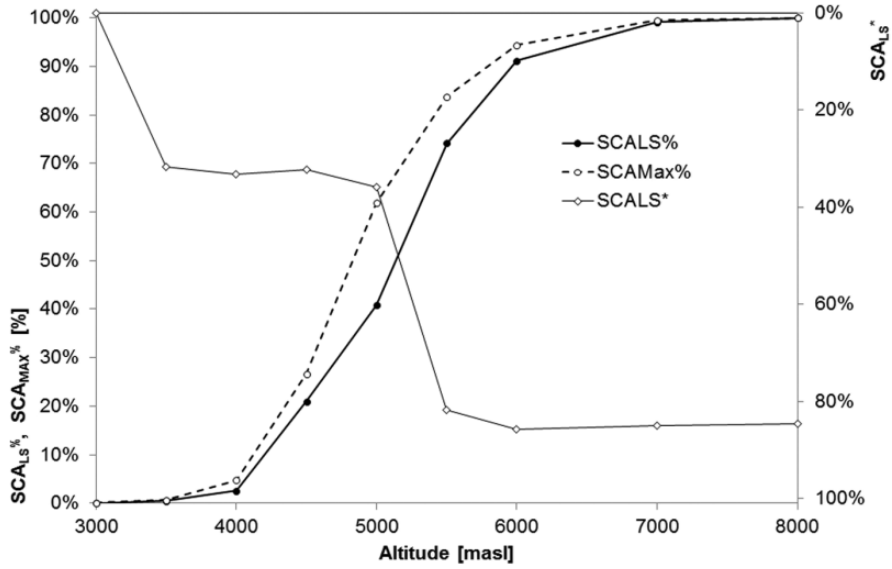

Figure 9. Distribution of 2001–2011 average snow covered area in altitude bins in late summer with respect to the whole area ($SCA_{LS}^{\%}$), of 2001–2011 average snow covered area in late summer (SCA_{LS}^{*}) with respect to greatest (maximum) snow covered area in that bin, and of the 2001–2011 greatest snow covered area in each bin with respect to the sum of 2001–2011 maximum values of snow covered areas in the whole park ($SCA_{Max}^{\%}$). Logarithmic scale (base 2) is used to enhance small snow covered areas at very low (and very high) altitudes. $SCA_{LS}^{\%}$: 2001–2011 average snow cover area in late summer, with respect to the whole snow cover area in late summer in the CKNP; SCA_{LS}^{*}: 2001–2011 average snow cover area in late summer; $SCA_{Max}^{\%}$: ratio of 2001–2011 greatest snow cover area in each bin to the 2001–2011 greatest snow cover areas in the whole CKNP.

Table 9. Characteristics of three elevation zones for snow cover with slope values from linear regression analysis upon average snow cover.

Zone	Altitude bin (m)	$Surface_{zone}$ (km^2)	Ave SCA ($km^2\ yr^{-1}$)	$Slope_{SCA}$ ($km^2\ yr^{-1}$)	$Slope_{SCA\%}$ (% yr^{-1})
A	1900–3300	845	4.6	0.1	2
B	3301–4300	2803	384.4	2.3	0.6
C	4301–8400	9551	6574.6	14.9	0.2
$A_{TOT}/Slope_{\%w}$		13200		17.3	0.25

Ave SCA: average snow covered area; $Slope_{SCA\%}$: slope weighted upon SCA.

of our climate analysis, the observed abundant supraglacial debris, and the role of the surging glaciers in the region. Then, accuracy and validation of our snow analysis is discussed, and finally, a comparison between our glacier inventory and the other existing inventories is presented.

I The relation between climate change and glacier stability in the CKNP

The analysis of climate data from 1980 to 2009 measured by three AWSs (Table 3) revealed that the occurrence of precipitation events has increased. Considering that the median elevation

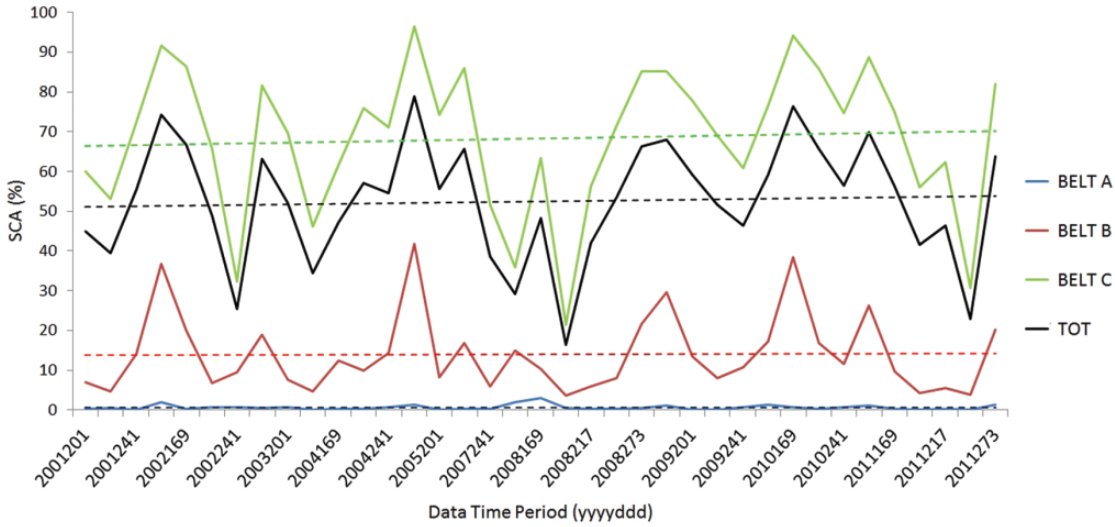

Figure 10. SCA values for three different altitudinal zones (A, B, C see Table 9) of the CKNP for the May–September window in 2000–2011. Data time period is given in years and Julian days.

of the CKNP glaciers is close to 5000 m, that the average minimum winter air temperature is below 0°C most of the time, and that most of the precipitation occurs in winter, this would translate into more frequent snowfalls. This assumption is confirmed by the analysis of the SCA variation, which revealed slightly increasing snow cover during the 2001–2010 ablation seasons in this area. This finding is in accordance with Hasson et al. (2014), who found that summer SCA increased on average during 2001–2012 in the Shigar basin, where most of the CKNP is located. Tahir et al. (2011) gave further evidence of increasing SCA in the upper Karakoram for the same period, while Gurung et al. (2011) reported rising SCA in the western HKH during 2002–2010.

The role of snow is of great importance for glacier preservation (especially during melt season), as snow reflects a large portion of the incoming solar radiation, protecting the underneath ice from melt. The same increasing trend in SCA is confirmed also between 5000 and 5500 m a.s.l., where (i) the greatest cumulated SCA loss (i.e., the vertical distance between $SCA_{LS}{}^{\%}$ and $SCA_{Max}{}^{\%}$, see Figure 9) is found; (ii) most of the glacier area resides (see Figure 2); and (iii) debris cover is sparse and can enhance ice melt.

A decreasing trend in summer mean air temperature was observed at Gilgit AWS during 1980–2009, and this would support snow and ice preservation during the ablation season. Evidences are also given by Shekhar et al. (2010), who found a decrease of $\sim$1.6°C and 3°C, respectively, in maximum and minimum air temperature over the Karakoram range during 1985–2007, while Hasson et al. (2015) found a significant cooling in July–October during 1995–2012 in the Upper Indus Basin. Quincey et al. (2009) found decreasing mean summer air temperatures modeled over the Baltoro area during 1958–2001. Gardelle et al. (2012) connected the reduced river runoff in the central Karakoram with decreasing ice and snow melt rates (as these would be the major water sources of rivers in this region, according to Immerzeel et al., 2010).

Finally, length and area changes are harder to interpret in climatic terms than mass changes, as

Table 10. Results of the climate trend analysis: (a) results of the LR and MK analysis. For MK, *p*-value is displayed. The LR values are the linear regression coefficients (i.e., slope of the regression line, unity/year), LR p corresponds to the *p*-value. In bold significant *p*-value ($\alpha = 5\%$) are given; (b) the beginning year and average values before and after the start for the trends derived from the progressive MK test are given. LT is the long term (1980–2009) average; (c) correlation analysis of station mean climatic variables vs global temperature anomalies ΔT_G and NAO index. The significant correlation ($p = 5\%$) results are displayed in bold.

(a) AWS	P_m-D_w	P_Y	P_{JFM}	P_{AMJ}	P_{JAS}	P_{OND}	D_{wY}	D_{wJFM}	D_{wAMJ}	D_{wJAS}	D_{wOND}
Astore	MK	0.38	0.40	0.60	0.90	0.56	0.25	0.96	0.66	0.10	0.71
Astore	LR_s	−2.22	−0.94	−0.39	0.00	−0.89	0.34	0.01	−0.01	0.08	0.03
Astore	LR_p	0.43	0.55	0.84	1.00	0.49	0.22	0.71	0.87	0.04	0.27
Bunji	MK	0.90	0.42	0.99	0.99	0.84	0.84	0.38	0.38	0.68	0.79
Bunji	LR_s	−0.32	0.29	−0.18	0.03	−0.47	−0.06	−0.01	−0.03	0.00	0.02
Bunji	LR_p	0.82	0.49	0.84	0.96	0.39	0.81	0.85	0.44	0.94	0.28
Gilgit	MK	0.42	0.87	0.40	0.79	0.90	0.00	0.00	0.15	0.21	0.93
Gilgit	LR_s	0.59	0.09	0.78	−0.07	−0.20	0.87	0.11	0.09	0.06	0.03
Gilgit	LR_p	0.55	0.80	0.34	0.87	0.64	0.00	0.00	0.04	0.12	0.38
AWS	T_{min}-T_{max}	T_Y	T_{JFM}	T_{AMJ}	T_{JAS}	T_{OND}	T_Y	T_{JFM}	T_{AMJ}	T_{JAS}	T_{OND}
Astore	MK	0.07	0.05	0.04	0.71	0.23	0.01	0.01	0.34	0.99	0.28
Astore	LR_s	0.03	0.05	0.06	0.00	0.02	0.04	0.08	0.05	0.01	0.04
Astore	LR_p	0.02	0.05	0.01	0.87	0.23	0.01	0.00	0.11	0.76	0.09
Bunji	MK	0.01	0.00	0.03	0.82	0.02	0.58	0.01	0.73	0.07	0.42
Bunji	LR_s	0.04	0.07	0.06	−0.01	0.04	0.01	0.06	0.01	−0.03	0.02
Bunji	LR_p	0.00	0.00	0.01	0.81	0.04	0.38	0.01	0.73	0.13	0.29
Gilgit	MK	0.16	0.42	0.76	0.03	0.49	0.00	0.00	0.33	0.93	0.01
Gilgit	LR_s	−0.01	0.02	0.01	−0.05	−0.02	0.05	0.09	0.06	0.00	0.07
Gilgit	LR_p	0.41	0.39	0.62	0.02	0.41	0.00	0.00	0.07	0.85	0.00
(b) AWS	Var.	Year st.	LT	Before	After	AWS	Var.	Year st.	LT	Before	After
Astore	T_{minJFM}	2002	−4.4	−4.8	−3.7	Bunji	T_{minOND}	1997	5.1	4.9	5.5
Astore	T_{minAMJ}	1999	7.6	7.2	8.4	Bunji	T_{maxJFM}	1997	13.8	13.3	14.5
Astore	T_{maxY}	1998	15.7	15.3	16.2	Gilgit	D_{wY}	2001	39.3	33.6	53.4
Astore	T_{maxJFM}	2000	5.4	4.8	6.4	Gilgit	T_{minJAS}	1986	15.6	16.7	15.3
Bunji	T_{minY}	2003	10.9	10.7	11.7	Gilgit	T_{maxY}	1995	24.1	23.7	24.6

(continued)

Table 10. (continued)

(a) AWS	P_m-D_w	P_Y	P_{JFM}	P_{AMJ}	P_{JAS}	P_{OND}	D_{wY}	D_{wJFM}	D_{wAMJ}	D_{wJAS}	D_{wOND}
Bunji	T_{minJFM}	1997	3.5	3.1	4.1	Gilgit	T_{maxJFM}	1995	13.8	13	14.6
Bunji	T_{minAMJ}	2001	15.3	15	16.2	Gilgit	T_{maxOND}	1991	18.9	18.2	19.3
(c)	Y	JFM	AMJ	JAS	OND	-	Y	JFM	AMJ	JAS	OND
$\Delta T_G/T_{min}$	0.21	0.25	0.35	−0.16	0.19	NAO/D_w	−0.32	−0.44	0.33	−0.33	−0.10
$\Delta T_G/T_{max}$	0.55	0.41	0.24	0.11	0.33	NAO/T_{min}	0.00	−0.36	−0.26	0.05	0.12
NAO/P_m	−0.14	0.10	0.17	0.18	0.17	NAO/T_{max}	−0.21	−0.23	−0.22	0.06	−0.05

LR: linear regression; MK: Mann–Kendal; ΔT_G: global temperature anomalies; D_W: wet days; NAO: North Atlantic Oscillation; JFM: January–February–March; AML: April–May–June; JAS: July–August–September; OND: October–November–December; Y: Year.

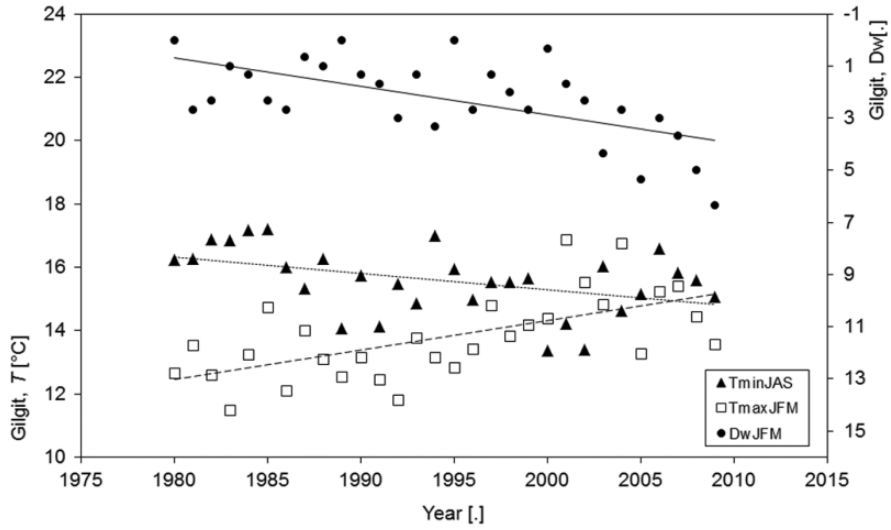

Figure 11. Summer (JAS) minimum air temperatures and winter (JFM) maximum air temperatures for the Gilgit AWS, including their linear trends. In addition, the number of wet days D_w during winter is also displayed.

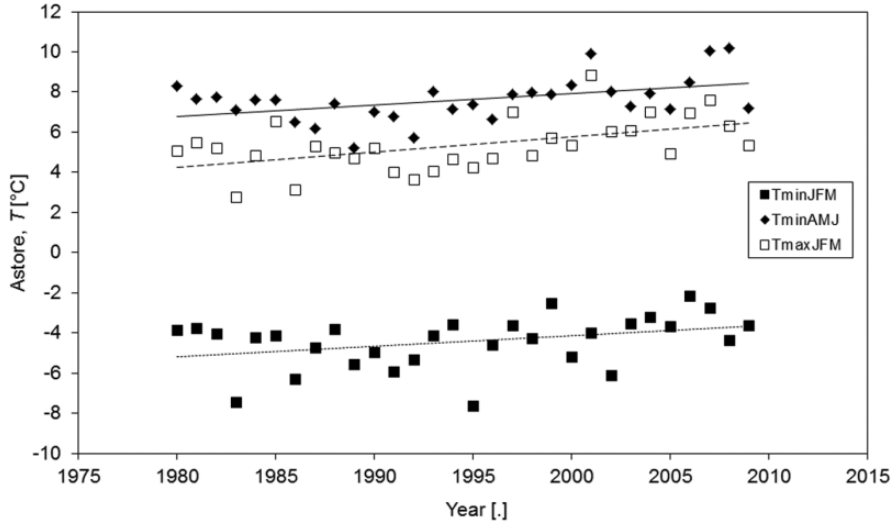

Figure 12. Seasonal minimum air temperatures (winter: JFM, spring: AMJ) and winter maximum air temperatures for the Astore AWS, including their linear trends.

they respond slower (and in some cases even not at all) to climate variations. Indeed, there is a delay of the glacier area response to climate change depending on glacier size, with usually longer response times for larger glaciers (Bolch et al., 2012). Glacier area gain may be the result of several decades of positive mass balance for large glaciers (Bhambri et al., 2013), which are frequent in the study area. The observed climate change towards more favorable conditions for

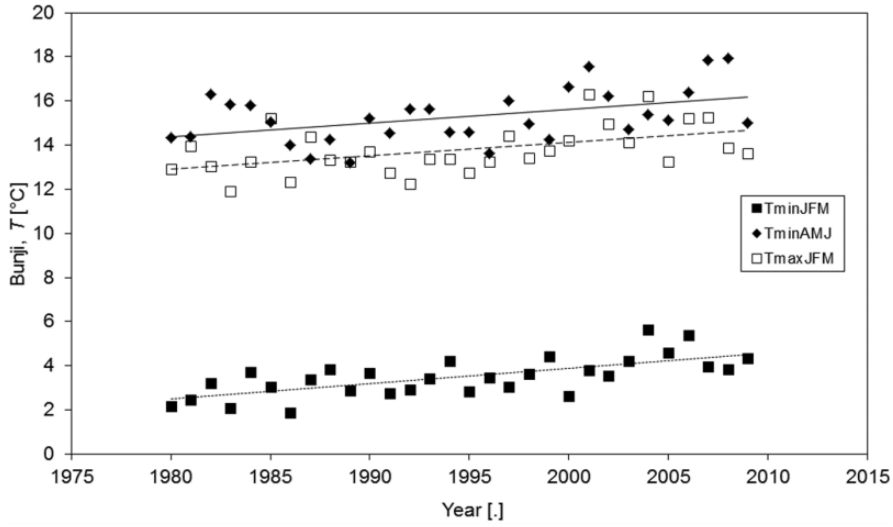

Figure 13. Seasonal minimum air temperatures (winter: JFM, spring: AMJ) and winter maximum air temperatures for the Bunji AWS, including their linear trends.

glaciers in the Karakoram seems to substantiate the slight glacier mass gain found by Gardelle et al. (2012, 2013) for the 1998–2008 period (equal to $+0.10 \pm 0.16$ m w.e. yr^{-1}). Either this mass change was not large enough to cause an increase of glacier surfaces in the region, or it occurred too recently, and glacier areas might respond in the future only to this changed condition.

2 Difference between debris-free and debris-covered glaciers in the CKNP

If CKNP glaciers are divided into debris-free and debris-covered types, we can immediately recognize two patterns. On the one hand, debris-covered glaciers are mostly larger—Baltoro, Biafo and Hispar glaciers belong to this group—and they reach the lowest elevations (even below 3000 m a.s.l., see Figure 3). Moreover, they are covered by debris almost entirely up to about 4000 m a.s.l. (see Figure 2). The debris can be brought by landslides from the steep rock-walls surrounding the glaciers, rock falls, and debris-laden snow avalanches. On the other hand, debris-free glaciers are in general smaller (the Yazghil Glacier being the largest with 87 km^2), and their termini are found higher up on average (4600 m a.s.l., almost 700 m above the mean termini of debris-covered glaciers) (Figure 14).

From our analysis, the presence of glaciers below 4000 m a.s.l. seems to be linked with the presence of a supraglacial debris cover. Debris can have two opposite effects on the ice (Diolaiuti et al., 2009; Østrem, 1959). If it is thick enough (more than a critical thickness, to be derived with field observations, Mattson et al., 1993), it decreases ice melt rates by reducing the heat flux from the top of the debris layer to the debris-ice interface (Bocchiola et al., 2010). According to Juen et al. (2014), a debris layer thicker than 0.1 m is able to diminish ablation efficiently, while Mihalcea et al. (2006) reported a critical debris thickness of around 0.05 m on the Baltoro Glacier. The debris thickness over most of the glacier termini in this region is very high (often >1 m, Copland et al., 2009; Mayer et al., 2006), and therefore is able to reduce ice melt and preserve glaciers

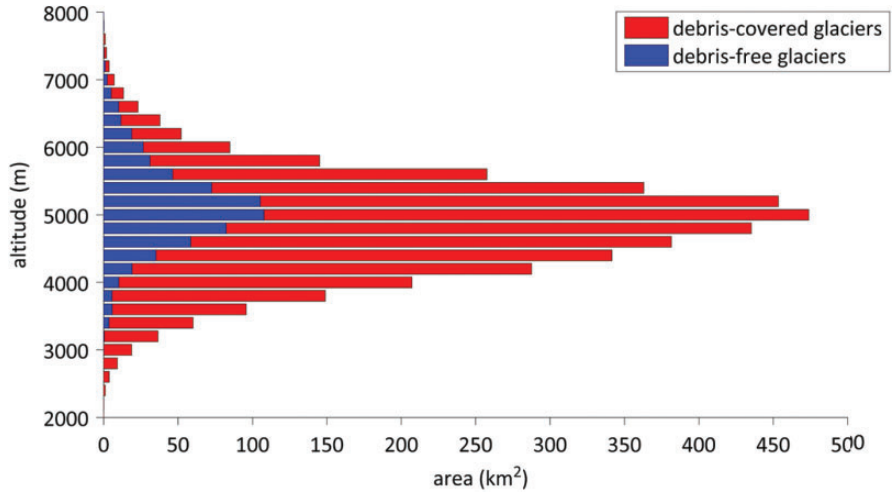

Figure 14. Debris-free and debris-covered glacier areas distribution per 200 m altitude bins.

at such low altitudes where temperatures are generally higher.

On the other hand, exposed ice cliffs and meltwater ponds, the presence of which is usually related to debris occurrence (Benn et al., 2012), can enhance ice ablation. Sakai et al. (2002) have shown that ice cliffs on glaciers in Nepal could make a large net contribution to total ablation of debris-covered glaciers, although covering a small percentage of the total glacier area. Juen et al. (2014) stated, however, that melt on ice cliffs plays a significant role for ice ablation, but not as high as concluded by Sakai et al. (1998). Reid and Brock (2014) concluded that ice cliffs (even the smallest ones) account for $\sim 7.4\%$ of the total ablation on the Miage Glacier. The effect of ice cliffs at a local scale can be clearly seen in patterns of glacier elevation change from DEM differencing (Bolch et al., 2011). However, Gardelle et al. (2012) found no significant differences in surface elevation change between debris-free and debris-covered glaciers in the Karakoram in the last decade, indicating that the Karakoram Anomaly likely is controlled by other factors than debris cover.

Finally, from Table 11 in Section V.3, we observe that debris-free and debris-covered glaciers contribution are similar but opposite, being the first positive and the second negative. Nevertheless, these area changes represent less than 1% of the glacier area of both categories. In Section V.3 we will see that most of the debris-free gain is due to surge advances.

3 The contribution of the surging events to the CKNP glacier area change

The total area of the CKNP glaciers was rather stable during 2001–2010 ($+0.4 \pm 202.9$ km^2 over about 4606 km^2). This value includes also the area gain due to surge activities. As a surge trigger mechanism remains inconclusive in the region and very likely is not directly driven by climate variations (Quincey and Luckman, 2014), we decided to split the analysis between surge- and non-surge-type glaciers. Neglecting the surge-type advances, the remaining glacier surface is still more or less stable. The contribution of the surge-type advances on the total area gain results to 28%. It is also worth to note that four out of eight surge-type glaciers are debris-free, and account for even 77% of the

Table 11. Glacier area variation divided into debris-free, debris-covered, and surge and non-surge type glaciers during 2001–2010. $\Delta A_{cov2001-2010}$ (%) is the percentage of area change relative to glacier coverage (debris-free, or -covered), for surge and non-surge area changes. $\Delta A_{rel2001-2010}$ (%) is the percentage of area change relative to the total change ($+0.4 \pm 202.9$ km^2 over about 4606 km^2), for debris-free and debris-covered glaciers. Mean elevation values are also given.

	Debris-free glaciers		Debris-covered glaciers		Total	
	no surge	only surge	no surge	only surge	debris-free	debris-covered
Glacier number	528	4	178	1	532	179
Glacier number (%)	74.3	0.6	25.0	0.1	74.8	25.2
2001 Area (km^2)	609.7 ± 7.7	50.8 ± 2.6	3940.5 ± 85.7	4.9 ± 0.8	660.5 ± 8.2	3945.4 ± 85.7
2010 Area (km^2)	610.7 ± 14.5	54.3 ± 6.4	3936.4 ± 183.0	5.0 ± 1.6	665.0 ± 15.9	3941.4 ± 183.0
$\Delta A_{2001-2010}$ (km^2)	$+1.0 \pm 16.5$	$+3.5 \pm 6.9$	-4.0 ± 202.1	$+0.1 \pm 1.8$	$+4.5 \pm 17.8$	-4.0 ± 202.1
$\Delta A_{2001-2010}$ (%)	+0.2	+0.5	−0.1	+0.002	+0.7	−0.1
$\Delta A_{cov2001-2010}$ (%)	+22.6	+77.4	−98.5	+1.5		
$\Delta A_{rel2001-2010}$ (%)					+52.8	−47.2
Mean altitude (m)	5029	5291	4864	5170	5031	4866

total area change of all the CKNP debris-free glaciers. It means that most of the area change from debris-free glaciers is due to surging. The most prominent surge example is the Shingchukpi Glacier, which is the debris-free glacier with the largest surge advance (2220 m). It is now in touch with the Panmah Glacier. On the other hand, the area change due to surge is negligible for debris-covered glaciers (Table 11).

Despite the relatively large length and area changes, and the high flow velocities during the active phase of a surge (up to 5 km yr^{-1} for the Khurdopin Glacier in the 1970s according to Quincey and Luckman, 2014), it is difficult to connect such advances to changes in mass balance. Previous works on surging glaciers in the Karakoram have suggested that climatically induced changes in glacier thermal conditions may be linked to observed exceptional surging (Hewitt, 2005), while others indicate that a change in subglacial drainage is the dominant control (Mayer et al., 2011). Quincey et al. (2011) speculated that recent surges in the Karakoram might be controlled by thermal rather than hydrological conditions, coinciding with high-altitude warming from long-term precipitation and accumulation patterns. Nevertheless, there is consensus that surge events are increasing in the Karakoram, and this is likely to reflect somehow recent changes in precipitation and temperature in the region (Hewitt, 2007; Copland et al., 2011; Bocchiola and Diolaiuti, 2013). Recently, Herreid et al. (2015), found no significant difference in the Hunza basin between surging and non-surging glaciers in terms of total glacier area in a period of 37 years on a sample of 93 glaciers. However, according to the present knowledge, surge-type glaciers might obscure the actual glacier response to climate change in this region—in particular because their return periods are poorly constrained (Quincey and Luckman, 2014)—and should therefore be discussed separately.

4 Comparison with the other glacier inventories

We compared our glacier outlines with the ICIMOD inventory (Bajracharya and Shrestha, 2011), and the Randolph Glacier Inventory, version 4.0 (RGI, Arendt et al., 2014), the two other region wide inventories. The source of the data used in the RGI 4.0 for our region is mainly the Global Land Ice Measurements from Space initiative

Table 12. Summary of glaciers in the CKNP glacier inventory (year 2001), ICIMOD inventory, and the RGI 4.0. The areas are compared with respect to the CKNP 2001 inventory (see "Difference" values). Only glacier polygons mapped in all the three inventories at the same time are shown.

	CKNP 2001	ICIMOD			RGI 4.0		
			Difference			Difference	
	Area (km^2)	Area (km^2)	(km^2)	(%)	Area (km^2)	(km^2)	(%)
Total area	4256.8 ± 63.9	4185.0	−71.8	−2	4658.5	401.7	9
above ELA	1342.9 ± 2.6	1573.2	230.3	17	1831.6	488.7	36

(GLIMS)—which consists mostly of data from the first Chinese Glacier Inventory (Shi et al., 2009)—but it also includes outlines from a previous ICIMOD inventory (Mool et al., 2007), and some from Bhambri et al. (2013) in the Shyok river basin. To make the comparison consistent, we selected only those glacier polygons which were mapped in all the three inventories at the same time. We chose to compare the outlines from 2001 of our inventory because they are closer in time to both the other inventories. The comparison was made for the entire glacier area and for the accumulation area only, because minor changes over time are expected to occur in the accumulation area. An elevation of 5200 m a.s.l. was used as ELA, for the reasons discussed in the Results chapter.

Table 12 shows the differences in area between the ICIMOD and the RGI inventories, compared to our mapping results. The relative area difference is not large with respect to the total glacier surface, but shows a tendency to higher values above the ELA. Our inventory tends to underestimate the glacier area in the accumulation zone. In particular, the difference in accumulation area amongst our inventory and the ICIMOD one is half the one found by comparing it with the RGI (version 4.0). This might derive from different strategies of mapping the upper glacier limits in the different inventories. In particular, the ICIMOD inventory used a slope criterion to exclude all the headwalls steeper than 60° from the upper glacier limit. This approach can partly explain the lower overall glacier area found in the ICIMOD inventory and the present one, compared to the RGI 4. Indeed, the inclusion of the steep headwalls of the accumulation basins in the glacier outlines, and the presence of seasonal snow cover in the source data, lead to larger glacier areas in the RGI, as also reported by Nuimura et al. (2015). These authors present a new glacier inventory (the GAMDAM glacier inventory, GGI) where they report significantly less glacier area compared to RGI 4.0 in the Karakoram region (-13%), and significantly more compared to ICIMOD (+22%). Unfortunately, we are not able to make a direct comparison with the GGI, as this is not available for download, and we cannot extract the glacier areas within the CKNP borders (which correspond to one third of the whole Karakoram glaciers, according to ICIMOD). We can only observe that our inventory is in-between the RGI and ICIMOD just like the GGI (Table 12).

Very recently, version 5 of the RGI was released, with a glacier area of 5593.7 km^2 in the study zone.

We overlapped the glacier outlines of all the available inventories by twos, and extracted the regions which did not match, to study the absolute differences between inventories (Table 13). From this analysis, the RGI gave results farthest from the other inventories in absolute terms. The greatest difference is found when comparing the accumulation zone, probably for the same reasons just discussed.

Table 13. Glacier areas and absolute differences between inventories. Only glaciers which were mapped in all the three inventories at the same time are considered. Percentages are calculated on the mean of the total area of the two inventories used for comparison.

		Total area	Above ELA
CKNP 2001	(km^2)	4256.8 $\pm$ 63.9	1342.9 $\pm$ 2.6
ICIMOD	(km^2)	4185.0	1573.2
RGI 4.0	(km^2)	4658.5	1831.6
ICIMOD-CKNP	(km^2)	1297.2	609.9
	(%)	31	42
CKNP-RGI	(km^2)	3014.9	1287.1
	(%)	68	81
ICIMOD-RGI	(km^2)	3056.9	1261.4
	(%)	69	74

VI Conclusions

The present manuscript exploits Landsat images to produce a detailed glacier inventory of the Central Karakoram National Park and to analyze the glacier changes during the first decade in the new millennium. It provides a dataset of glacier boundaries for 711 glaciers for the years 2001 and 2010. A supervised classification on the Landsat images allowed the spatial analysis of the supraglacial debris, which is abundant in the glacier ablation area ($\sim$31% coverage). Debris covers most of the glacier area up to 4000 m and its thickness is very high at the terminus (up to >1 m, Copland et al., 2009; Mayer et al., 2006; Minora et al., 2015).

The analysis of the area changes during 2001–2010 reveals a general stability (+0.4 $\pm$ 202.9 km^2 over 4605.9 $\pm$ 86.1 km^2 in 2001), evidence of the anomalous behavior of glaciers in the Karakoram in contrast to a worldwide shrinkage of mountain glaciers. Even when neglecting the surge-type advances, the area change remains stable, but is slightly negative. However, the abundance of surge type glaciers plays an additional role in transporting ice volume towards lower altitudes.

The Karakoram Anomaly is analyzed in view of the ongoing climate change. A slight increase in late summer SCA during 2001–2010 is observed from MODIS snow data. At the same time, the available weather stations reveal an increase of snowfall events and a decrease of mean summer air temperatures since 1980, which would translate into more persistent snow cover during the melt season. These results support an enhanced glacier preservation in the ablation areas due to a long-lasting snow cover, and stronger accumulation at higher altitudes, pushing towards positive net balances. Nevertheless, linking these observations to the analysis of glacier area changes is not unambiguous, since there is a delay of the glacier area response to climate change depending on glacier size, with usually longer response times (even several decades) for larger glaciers (Bolch et al., 2012).

Finally, we stress the need to study the contribution of meltwater ponds and steep exposed ice cliffs to the overall ablation of Karakoram glaciers, to improve the understanding of the glacier melting processes in this region, as ice melt in the flat lower part of the glacier tongues represents a major source of water from the Karakoram watersheds to the Indus river.

Acknowledgements

Landsat data used in this paper are distributed by the Land Processes Distributed Active Archive Center (LP DAAC), located at USGS/EROS, Sioux Falls, SD. Climate data were kindly provided by PMD (Pakistan Meteorological Department). The CKNP glacier database is part of the SHARE GEO Network and data are available upon request to Ev-K2-CNR headquarter. Please visit the site http://geonetwork.evk2cnr.org.

Declaration of conflicting interests

The authors declared no potential conflicts of interest with respect to the research, authorship, and/or publication of this article.

Funding

The authors disclosed receipt of the following financial support for the research, authorship, and/or publication of this article: This research was performed under the umbrella of SEED and SHARE-PAPRIKA projects. SEED is a project funded by Pakistani and Italian governments, and managed by Ev-K2-CNR. SHARE-PAPRIKA is a project funded and managed by Ev-K2-CNR (it is the twin project of the PAPRIKA France program).

References

Aggarwal PK, Joshi PK, Ingram JSI, et al. (2004) Adapting food systems of the Indo-Gangetic plains to global environmental change: key information needs to improve policy formulation. *Environmental Science & Policy* 7(6): 487–498.

Akhtar M, Ahmad N and Booij MJ (2008) The impact of climate change on the water resources of Hindukush-Karakoram-Himalaya region under different glacier coverage scenario. *Journal of Hydrology* 355(1–4): 148–163.

Archer DR (2003) Contrasting hydrological regimes in the upper Indus Basin. *Journal of Hydrology* 274(1–4): 198–210.

Archer DR and Fowler HJ (2004) Spatial and temporal variations in precipitation in the Upper Indus Basin, global teleconnections and hydrological implications. *Hydrology and Earth System Sciences* 8(1): 47–61.

Arendt A, Bliss A, Bolch T, et al. (2014) *Randolph Glacier Inventory – A Dataset of Global Glacier Outlines: Version 4.0*. Boulder, CO: Global Land Ice Measurements from Space.

Bajracharya SR and Shrestha B (eds) (2011) *The Status of Glaciers in the Hindu Kush-Himalayan Region*. Kathmandu: ICIMOD.

Barrand N and Murray T (2006) Multivariate controls on the incidence of glacier surging in the Karakoram Himalaya. *Arctic, Antarctic, and Alpine Research* 38(4): 489–498.

Belò M, Mayer C, Lambrect A, et al. (2008) The recent evolution of Liligo Glacier Karakoram, Pakistan and its present quiescent phase. *Annals of Glaciology* 48(1): 171–176.

Benn DI, Bolch T, Hands K, et al. (2012) Response of debris-covered glaciers in the Mount Everest region to recent warming, and implications for outburst flood hazards. *Earth-Science Reviews* 114(1–2): 156–174.

Bhambri R, Bolch T, Chaujar RK, et al. (2011) Glacier changes in the Garhwal Himalaya, India, from 1968 to 2006 based on remote sensing. *Journal of Glaciology* 57(203): 534–556.

Bhambri R, Bolch T, Kawishwar P, et al. (2013) Heterogeneity in glacier response in the upper Shyok valley, northeast Karakoram. *The Cryosphere* 7: 1385–1398.

Bocchiola D, Bianchi JE, Gorni E, et al. (2008) Regional evaluation of three day snow depth frequency curves for Switzerland. *NHESS* 8: 685–705.

Bocchiola D (2014) Long term (1921–2011) hydrological regime of Alpine catchments in Northern Italy. *Advances in Water Resources* 70: 51–64.

Bocchiola D and Diolaiuti GA (2013) Recent (1980–2009) evidence of climate change in the upper Karakoram, Pakistan. *Theoretical and Applied Climatology* 113(3–4): 611–641.

Bocchiola D, Diolaiuti GA,, Soncini A, et al. (2011) Prediction of future hydrological regimes in poorly gauged high altitude basins: the case study of the upper Indus, Pakistan. *Hydrology and Earth System Sciences* 15(7): 2059–2075.

Bocchiola D, Mihalcea C, Diolaiuti GA, et al. (2010) Flow prediction in high altitude ungauged catchments: a case study in the Italian Alps (Pantano Basin, Adamello Group). *Advances in Water Resources* 33(10): 1224–1234.

Bolch T, Kulkarni A, Kääb A, et al. (2012) The state and fate of Himalayan glaciers. *Science* 336(6079): 310–314.

Bolch T, Pieczonka T and Benn DI (2011) Multi-decadal mass loss of glaciers in the Everest area (Nepal Himalaya) derived from stereo imagery. *The Cryosphere* 5: 349–358.

Bookhagen B and Burbank DW (2010) Towards a complete Himalayan hydrologic budget: the spatiotemporal distribution of snow melt and rainfall and their impact on river discharge. *Journal of Geophysical Research* 115: F03019.

Braithwaite R and Raper S (2009) Estimating equilibrium-line altitude (ELA) from glacier inventory data. *Annals of Glaciology* 50(53): 127–132.

Brohan P, Kennedy JJ, Harris I, et al. (2006) Uncertainty estimates in regional and global observed temperature changes: a new dataset from 1850. *Journal of Geophysical Research* 111: D12106.

CGIAR-CSI (2012) Consortium for Spatial Information. Available at: www.cgiar-csi.org (accessed 20 February 2014).

Citterio M, Diolaiuti GA, Smiraglia C, et al. (2007) The fluctuations of Italian glaciers during the last century: a contribution to knowledge about Alpine glacier changes.

Geografiska Annaler Series A: Physical Geography 89(3): 164–182.

Cogley JG (2009) Geodetic and direct mass-balance measurements: comparison and joint analysis. *Annals of Glaciology* 50(50): 96–100.

Copland L, Sharp MJ and Dowdeswell JA (2003) The distribution and flow characteristics of surge-type glaciers in the Canadian High Arctic. *Annals of Glaciology* 36(1): 73–81.

Copland L, Pope S, Bishop MP, et al. (2009) Glacier velocities across the central Karakoram. *Annals of Glaciology* 50(52): 41–49(9).

Copland L, Sylvestre T, Bishop MP, et al. (2011) Expanded and recently increased glacier surging in the Karakoram. Institute of Arctic and Alpine Research (INSTAAR), University of Colorado. Available at: www.bioone.org/doi/full/10.1657/1938-4246-43.4.503 (accessed 17 October 2015).

Cuffey KM and Paterson WSB (2010) *The Physics of Glaciers*. 4th ed. Oxford: Pergamon Press.

Diolaiuti GA, Bocchiola D, Vagliasindi M, et al. (2012) The 1975-2005 glacier changes in Aosta Valley (Italy) and the relations with climate evolution. *Progress in Physical Geography* 36(6): 764–785.

Diolaiuti GA, D'Agata C, Meazza A, et al. (2009) Recent (1975–2003) changes in the Miage debris-covered glacier tongue (Mont Blanc, Italy) from analysis of aerial photos and maps. *Geografia Fisica e Dinamica Quaternaria* 32: 117–127.

Diolaiuti GA, Pecci M and Smiraglia C (2003) Liligo Glacier (Karakoram): reconstruction of the recent history of a surge-type glacier. *Annals of Glaciology* 36(1): 168–172.

Falorni G, Teles V, Vivoni ER, et al. (2005) Analysis and characterization of the vertical accuracy of digital elevation models from the Shuttle Radar Topography Mission. *Journal Of Geophysical Research* 110: F2. DOI:10.1029/2003JF000113.

Fowler HJ and Archer DR (2006) Conflicting signals of climatic change in the Upper Indus basin. *Journal of Climate* 19: 4276–4293.

Gardelle J, Berthier E and Arnaud Y (2012) Slight mass gain of Karakoram glaciers in the early 10 twenty-first century. *Nature Geoscience* 5: 322–325.

Gardelle J, Berthier E, Arnaud Y, et al. (2013) Region-wide mass balances over the Pamir-Karakoram-Hiimalaya during 1999–2011. *The Cryosphere* 7: 1263–1286.

Gardner AS, Moholdt G, Cogley JG, et al. (2013) A reconciled estimate of glacier contributions to sea level rise: 2003 to 2009. *Science* 340(6134): 852–857.

Gurung DR, Amarnath G, Khun SA, et al. (2011) *Snow-Cover Mapping and Monitoring in the Hindukush-Himalayas*. Kathmandu: ICIMOD.

Hall DK, Salomonson VV and Riggs GA (2006) *MODIS/Terra Snow Cover 8-Day L3 Global 500 m Grid*. Version 5. Boulder, CO: National Snow and Ice Data Center.

Hasson S, Böhner J and Lucarini V (2015) Prevailing climatic trends and runoff response from Hindukush-Karakoram-Himalaya, upper Indus basin. *Earth System Dynamics Discussions* 6: 579–653.

Hasson S, Lucarini V, Khan M, et al. (2014) Early 21st century snow cover state over the western river basins of the Indus River system. *Hydrology and Earth System Sciences* 18: 4077–4100.

Herreid S, Pellicciotti F, Ayala A, et al. (2015) Satellite observations show no net change in the percentage of supraglacial debris-covered area in northern Pakistan from 1977 to 2014. *Journal of Glaciology* 61(227): 524–536.

Hewitt K (2005) The Karakoram Anomaly? Glacier expansion and the "elevation effect", Karakoram Himalaya. *Mountain Research and Development* 25(4): 332–340.

Hewitt K (2007) Tributary glacier surges: an exceptional concentration at Panmah Glacier, Karakoram, Himalaya. *Journal of Glaciology* 53(181): 181–188.

Hewitt K (2011) Glacier change, concentration, and elevation effects in the Karakoram Himalaya, Upper Indus Basin. *Mountain Research and Development* 31(3): 188–200.

Hurrell JW (1995) Decadal trends in the North Atlantic Oscillation regional temperatures and precipitation. *Science* 269(5224): 676–679.

Immerzeel WW, Van Beek LPH and Bierkens MFP (2010) Climate change will affect the Asian water towers. *Science* 328(5984): 1382–1385.

Jiang T, Su B and Hartmann H (2007) Temporal and spatial trends of precipitation and river flow in the Yangtze River Basin, 1961–2000. *Geomorphology* 85(3–4): 143–154.

Jones PD, Jonsson T and Wheeler D (1997) Extension to the North Atlantic Oscillation using early instrumental pressure observations from Gibraltar and south-west Iceland. *International Journal of Climatology* 17: 1433–1450.

Juen M, Mayer C, Lambrecht A, et al. (2014) Impact of varying debris cover thickness on ablation: a case study for Koxkar Glacier in the Tien Shan. *The Cryosphere* 8: 377–386.

Kääb A, Berthier E, Nuth C, et al. (2012) Contrasting patterns of early twenty-first-century glacier mass change in the Himalayas. *Nature* 488: 495–498.

Kääb A, Paul F, Maisch M, et al. (2002) The new remote sensing derived Swiss glacier inventory: II. First results. *Annals of Glaciology* 34(1): 362–366.

Kahlown MA, Raoof A, Zubair M, et al. (2007) Water use efficiency and economic feasibility of growing rice and wheat with sprinkler irrigation in the Indus Basin of Pakistan. *Agricultural Water Management* 87(3): 292–298.

Kendall MG (1975) *Rank Correlation Methods*. New York: Oxford University Press.

Manley WF (2005) Geospatial inventory and analysis of glaciers: a case study for the Eastern Alaska Range. In: Williams RS Jr and Ferrigno JG (eds) *Satellite Image Atlas of Glaciers of the World*. Professional Paper 1386-K. US Geological Survey, K424-K439.

Mann H B (1945) Nonparametric tests against trend. *Econometrica* 13: 245–259.

Mattson LE, Gardner JS and Young GJ (1993) Ablation on debris covered glaciers: an example from the Rakhiot Glacier, Punjab, Himalaya. In: *Proceedings of symposium on snow and glacier hydrology* (ed GJ Young), Kathmandu, November 1992, 289–298. IAHS Publication no. 218. Wallingford, UK: IAHS Publishing.

Mayer C, Fowler AC, Lambrecht A, et al. (2011) A surge of North Gasherbrum Glacier, Karakoram, China. *Journal of Glaciology* 57(205): 904–916.

Mayer C, Lambrecht A, Belò M, et al. (2006) Glaciological characteristics of the ablation zone of Baltoro Glacier, Karakoram. *Annals of Glaciology* 43(1): 123–131.

Mayer C, Lambrecht A, Mihalcea C, et al. (2010) Analysis of glacial meltwater in Bagrot Valley, Karakoram. *Mountain Research and Development* 30(2): 169–177.

Mihalcea C, Mayer C, Diolaiuti GA, et al. (2006) Ice ablation and meteorological conditions on the debris covered area of Baltoro Glacier (Karakoram, Pakistan). *Annals of Glaciology* 43: 292–300.

Mihalcea C, Mayer C, Diolaiuti GA, et al. (2008) Spatial distribution of debris thickness and melting from remote-sensing and meteorological data, at debris-covered Baltoro glacier, Karakoram, Pakistan. *Annals of Glaciology* 48(1): 49–57.

Minora U, Senese A, Bocchiola D, et al. (2015) A simple model to evaluate ice melt over the ablation area of glaciers in the Central Karakoram National Park, Pakistan. *Annals of Glaciology* 56(70): 202–216.

Mool PK, Bajracharya SR, Shrestha B, et al. (2007) Inventory of glaciers, glacial lakes and the identification of potential glacial lake outburst floods (GLOFs) affected by global warming in the mountains of Himalayan Region. Report, International Centre for Integrated Mountain Development, Kathmandu, Nepal.

Nuimura T, Sakai A, Taniguchi K, et al. (2015) The GAMDAM glacier inventory: a quality-controlled inventory of Asian glaciers. *The Cryosphere* 9: 849–864.

NSIDC (2013) National Snow and Ice Data Center. Available at: http://nsidc.org (accessed on 13 March 2014).

O'Gorman L (1996) Subpixel precision of straight-edged shapes for registration and measurement. *IEEE Transactions on Pattern Analysis and Machine Intelligence* 18(7): 746–751.

Osborn TJ (2004) Simulating the Winter North Atlantic Oscillation: the roles of internal variability and greenhouse gas forcing. *Climate Dynamics* 22(6): 605–623.

Osborn TJ (2006) Recent variations in the Winter North Atlantic Oscillation. *Weather* 61: 353–355.

Østrem G (1959) Ice melting under a thin layer of moraine, and the existence of ice cores in moraine ridges. *Geografiska Annaler* 41(4): 228–230.

Parajka J and Blöschl G (2008) The value of MODIS snow cover data in validating and calibrating conceptual hydrologic models. *Journal of Hydrology* 358(3–4): 240–258.

Paul F, Barrand NE, Baumann S, et al. (2013) On the accuracy of glacier outlines derived from remote-sensing data. *Annals of Glaciology* 54(63): 171–182.

Paul F, Barry RG, Cogley JG, Frey H, et al. (2009) Recommendations for the compilation of glacier inventory data from digital sources. *Annals of Glaciology* 50(53): 119–126.

Paul F, Huggel C and Kääb A (2004) Combining satellite multispectral data and a digital elevation model for mapping debris-covered glaciers. *Remote Sensing of Environment* 89(4): 510–518.

Pu Z, Xu L and Salomonson VV (2007) MODIS/Terra observed seasonal variations of snow cover over the Tibetan Plateau. *Geophysical Research Letters* 34: L06706.

Quincey DJ and Luckman A (2014) Brief communication: on the magnitude and frequency of Khurdopin glacier surge events. *The Cryosphere* 8: 571–874.

Quincey DJ, Braun M, Glasser NF, et al. (2011) Karakoram glacier surge dynamics. *Geophysical Research Letters* 38: L18504.

Quincey DJ, Copland L, Mayer C, et al. (2009) Ice velocities and climate variations for Baltoro Glacier, Pakistan. *Journal of Glaciology* 55(194): 1061–1071.

Racoviteanu AE, Arnaud Y, Williams MW, et al. (2008) Decadal changes in glacier parameters in the Cordillera Blanca, Peru, derived from remote sensing. *Journal of Glaciology* 54(186): 499–510.

Rankl M, Kienholz C and Braun M (2014) Glacier changes in the Karakoram region mapped by multimission satellite imagery. *The Cryosphere* 8: 977–989.

Reid TD and Brock BW (2014) Assessing ice-cliff backwasting and its contribution to total ablation of debris-covered Miage glacier, Mont Blanc massif, Italy. *Journal of Glaciology* 60(219): 3–13.

Sakai A, Nakawo M and Fujita K (1998) Melt rate of ice cliffs on the Lirung Glacier, Nepal Himalayas, 1996. *Bulletin of Glacier Research* 16: 57–66.

Sakai A, Nakawo M and Fujita K (2002) Distribution characteristics and energy balance of ice cliffs on debris-covered glaciers Nepal Himalaya. *Arctic*, *Antarctic, and Alpine Research* 34(1): 12–19.

Salerno F, Buraschi E, Bruccoleri D, et al. (2008) Glacier surface-area changes in Sagarmartha national park, Nepal, in the second half of the 20th century, by comparison of historical maps. *Journal of Glaciology* 54(187): 738–752.

Seidou O and Ouarda TBMJ (2007) Recursion-based multiple changepoint detection in multiple linear regression and application to river stream flows. *Water Resources Research* 43(7): W07404.

Shekhar MS, Chand H, Kumar S, et al. (2010) Climate-change studies in the western Himalaya. *Annals of Glaciology* 51(54): 105–112.

Scherler D, Bookhagen B and Srecker Manfred R (2011) Spatially variable response of Himalayan glaciers to climate change affected by debris cover. *Nature Geoscience* 4(3): 156–159.

Shi YF, Liu CH and Kang ES (2009) The glacier inventory of China. *Annals of Glaciology* 50(53): 1–4.

Shukla A, Arora MK and Gupta RP (2010) Synergistic approach for mapping debris-covered glaciers using optical–thermal remote sensing data with inputs from geomorphometric parameters. *Remote Sensing of Environment* 114(7) : 1378–1387.

Soncini A, Bocchiola D, Confortola G, et al. (2015). Future hydrological regimes in the upper Indus basin: a case study from a high altitude glacierized catchment. *Journal of Hydrometeorology* 16(1): 306–326.

Tahir AA, Chevallier P, Arnaud Y, et al. (2011) Snow cover dynamics and hydrological regime of the Hunza River basin, Karakoram Range, Northern Pakistan. *Hydrology and Earth System Sciences* 15: 2275–2290.

Tahir AA, Chevallier P, Arnaud Y, et al. (2011) Modeling snowmelt-runoff under climate scenarios in the Hunza River basin, Karakoram Range, Northern Pakistan. *Journal of hydrology* 409(1–2): 104–117.

Vaughan DG, Comiso JC, Allison I, et al. (2013) Observations: cryosphere. In: Stocker TF, Qin D, and Plattner GK, et al. (eds) *Climate Change 2013: The Physical Science Basis*. Contribution of Working Group I to the Fifth Assessment Report of the Intergovernmental Panel on Climate Change. Cambridge: Cambridge University Press.

Vögtle T and Schilling KJ (1999) Digitizing maps. In: Bähr H-P and Vögtle T (eds) *GIS for Environmental Monitoring*. Stuttgart, Germany: Schweizerbart, 201–216.

Wake CP, Mayewski PA and Spencer MJ (1990) A review of central Asian glaciochemical data. *Annals of Glaciology* 14: 301.

Wang X, Xie H and Liang T (2008) Evaluation of MODIS snow cover and cloud mask and its application in Northern Xinjiang, China. *Remote Sensing of Environment* 112: 1497–1513.

Weiers S (1995) Zur Klimatologie des NW-Karakoram und angrenzender Gebiete. Statistische Analysen unter Einbeziehung von Wettersatellitenbildern und eines Geographischen Information systems (GIS). *Bonner Geographische Abhandlungen* 92. Bonn, Germany: Geographisches Institut, Universität Bonn.

WGMS (2013) *Fluctuations of Glaciers Database*. Zurich, Switzerland: World Glacier Monitoring Service. Available at: http://dx.doi.org/10.5904/wgms-fog-2014-09 (accessed on 14 April 2014).

Winiger M, Gumpert M and Yamout H (2005) Karakoram-Hindukush-Western Himalaya: assessing high-altitude water resources. *Hydrological Processes* 19(12): 2329–2338.

Wulf H, Bookhagen B and Scherler D (2010) Seasonal precipitation gradients and their impact on fluvial sediment flux in the Northwest Himalaya. *Geomorphology* 118(1–2): 13–21.

Yao T, Thompson LG, Yang W, et al. (2012) Different glacier status with atmospheric circulations in Tibetan Plateau and surroundings. *Nature Climate Change* 2: 663–667.

Yue S and Wang CY (2002) Applicability of prewhitening to eliminate the influence of serial correlation on the Mann–Kendall test. *Water Resources Research* 38(6): 1068.

Zhang X, Vincent LA, Hogg WD, et al. (2000) Temperature and precipitation trends in Canada during the 20th century. *Atmosphere Ocean* 38(3): 395–429.